B isotope variations at variable scales in arc volcanoes: a case study of lavas from Paniri and Toconce, Northern Chile

Sinethemba Ncetani
NCTSIN001

Supervisor: Dr Petrus le Roux
Co-Supervisor: Dr Osvaldo González-Maurel

University of Cape Town
Department of Geological Sciences

Acknowledgements

The completion of this MSc. would not have been possible without consistent encouragements, prayers, and support of many people who were there for me when I did not feel encouraged to finish this project. I am eternally grateful to have you in my life.

I would like to express my deepest gratitude to my primary supervisor, Dr. Petrus le Roux, for his invaluable guidance, unwavering support, and endless patience throughout the entire research process. To my co-supervisor, Dr. Osvaldo González-Maurel, for his insightful feedback, patient support and very constructive criticism. His understanding of the Andean geology was especially instrumental in shaping my understanding of my study area. Their expertise and mentorship were instrumental in shaping this thesis, and a paragraph cannot do any justice in expressing my thanks.

Special thanks to our collaborators in Chile, Agradezco la oportunidad de trabajar con usted y gracias por su amabilidad y hospitalidad. Chile siempre tendrá un lugar especial en mi corazón. Dr Benigno Godoy thank you for your insightful feedback to my many questions and our field trip to the magical Andeas. Dr Dieter Garbe-Schönberg thank you for preparing our pressed nano-pellets for analyses. To the technical stuff at the UCT Department of Geological Sciences who helped with the preparation and analysis of samples, I am grateful for your assistance.

Without the financial support from SLR Consulting (South Africa) Ltd, the NRF, and Proyecto FONDECYT Iniciación n°11200013 this project would not have been possible.

I could list a lot of people who offered me both emotional and financial support during my pursuit of this MSc project. To my family and friends, I am grateful for your love, your kindness, your patience with my hard head, and your unwavering support. I love you! To uSiyabulela, Thandile, Landisiwe, Langalethu, Hlomla, Zendaya, I finished this work to show you that there is nothing in this world that is too big to dream of achieving. I am extremely confident that you can do way more than I have been able to do.

I dedicate this work to my Mother, Thobeka Ncetani, who went to be with her Lord 13yrs ago. Thobeka you missed out on a lot, I will forever carry your memory where ever I go.

LORD, you establish peace for us; all that we have accomplished you have done for us.

Abstract

The mountain building process witnessed today at the Andes is a good modern example of oceanic-continental convergence, providing a modern-day analogue that can be used to interpret older converging mountain belts around the world. Paniri (22°03'34"S, 68°13'42"W) a Pleistocene age stratovolcano and Toconce (22°11'17''S, 68°04'43''W) a late Pleistocene-Holocene age stratovolcano form part of the San Pedro-Linzor Volcanic Chain (SPLVC) that extends between 21°53'S 68°23'W and 22°09'S 67°58'W, located within the Altiplano-Puna Volcanic Chain (APVC), in the Central Andes of Northern Chile. Arc magmas have been widely established as good transporters of elements from the subducted oceanic slab in subduction zones. Boron (B) is an ideal geochemical tracer for the hydration of the overlying mantle wedge at subduction zones. The boron isotope composition of magmas is useful in detecting and quantifying the exchange process between the slab and the mantle. This is due to the large boron isotopic difference between the subducting altered oceanic crust and the mantle, and boron showing strong affinity for silicate melts and aqueous fluids. However, there are no investigations of B isotope systematics of **all** the units of a single stratovolcano. With B isotope data becoming more accessible due to advances in analytical methods, this study is timely in investigating B isotope systematics within volcanic centres and the regional significance.

To provide a firm geochemical framework for the interpretation of compositions in these volcanoes, new O isotope data were collected to complement existing data. The new $\delta^{18}O$ values at Paniri (7.69-8.82‰) and Toconce (9.63-10.91‰) overlap with available Andean lava $\delta^{18}O$ values and are significantly higher than mantle values of 5.5 to 5.9‰. Paniri and Toconce show increasing $\delta^{18}O$ values with increasing $^{87}Sr/^{86}Sr$ ratios (0.7055-0.7094 range over the SPLVC), and this correlation is indicative of magmas with increased contamination of the parent magma progressively towards the centre of the APMB as was previously observed on a regional scale.

New whole-rock boron concentrations and isotope ($\delta^{11}B$) values of samples from ***all*** 7 eruptive units at Paniri and from ***all*** 5 eruptive units at Toconce are presented, a unique boron dataset for stratovolcanoes. Paniri B contents range from 20 to 50(ppm) with $\delta^{11}B$ values from -6.11‰ (±0.35‰) to +0.23‰ (±0.33‰), and Toconce B values range from 19.71 to 83.5(ppm) with $\delta^{11}B$ from -11.16‰ (±0.36‰) to -5.06‰ (±0.49‰); both overlapping the range of boron values observed within the Andes. The elevated $\delta^{11}B$

values relative to the mantle value of approximately -10‰ support the influence of a more ^{11}B-enriched source like the altered oceanic crust (AOC). Between eruptive units: the older units have more depleted $\delta^{11}B$ values when compared to the younger eruptive units at both Paniri and Toconce. Within single eruptive units at Toconce (only one sample per unit was accessible at Paniri): distal samples have depleted $\delta^{11}B$ values compared to samples recovered more proximal to the volcanic vent. This suggest that first erupted lavas assimilated most of the ^{11}B-depleted crustal material locally available, with lava $\delta^{11}B$ compositions trending towards basement granitoids and metasediments $\delta^{11}B$ values (-11 ‰ to -5 ‰). With continued eruption, lavas progressively contain more ^{11}B-enriched values reflecting parental magma compositions of mantle wedge plus AOC (+3.4‰). The local, crustal, ^{11}B-depleted component is therefore not abundant and continued assimilation by successive magmas quickly cause local depletion.

A previously proposed two-step process leading to regional B variations in the Central Andes was found to agree with localised Paniri and Toconce data: (1) ^{11}B-rich AOC-derived fluids are mixed with a MORB-like mantle wedge resulting in parental melts of arc magmas with high $\delta^{11}B$ values; and, (2) the parental magmas now enriched in ^{11}B continued to ascend through the thick continental crust and APMB, with ~20-30% crustal assimilation at Paniri and 25-45% at Toconce leading to a decrease of the magma $\delta^{11}B$ composition while continuing to increase the $^{87}Sr/^{86}Sr$ ratios. There is a progressive increase in contamination with geographic location when moving from Paniri at the edges of the APMB to Toconce which is closer to the centre of the APMB.

This proposed process model agrees with the independently determined degrees of assimilation derived from O-Sr isotope systematics.

Contents

Acknowledgements 1
Abstract 2
Contents 4
1. Introduction 8
1.1. Arc Magmatism 8
1.2. Boron isotopes in volcanic arc settings 10
1.3. Objectives/aims of study: 12
2. Geological context 14
2.1. Regional geological context 14
2.1.1. The Andean Cordillera 14
2.1.2. Central Volcanic Zone 15
2.1.3. Altiplano-Puna Volcanic Complex 17
2.1.4. Altiplano-Puna Magmatic Body 18
2.2. Local geological context 19
2.2.1. San Pedro-Linzor Volcanic Chain (SPLVC) 19
2.2.2. Paniri Volcano 24
2.2.3. Toconce Volcano 28
3. Methods 30
3.1. Sample selection and preparation 30
3.2. X-Ray Fluorescence (XRF) 30
3.3. MC-ICP-MS 31
3.4. Laser fluorination 32
3.5. LA ICP-MS for trace elements in nano-pellets 33
3.6. LA MC-ICP-MS for B-isotopes in nano-pellets 33
4. Results 35
4.1. Major and Trace Element data 35
4.2. Isotope Analyses 42
5. Discussion 46
5.1. Contamination processes 46
5.2. B contents and $\delta^{11}B$ values in the Central Andes 49
5.3. New B contents and $\delta^{11}B$ values overview at Paniri and Toconce 52
5.4. Regional context for B isotope systematics in Paniri and Toconce 62
6. Conclusions 64
7. References 67

List of tables

Table 1(a): New major element XRF data for Toconce obtained from nano-pellet analysis, and existing major element XRF data for Paniri.....37

Table 2: New LA-ICP-MS trace element data (ppm) for Toconce samples obtained from nano-pellet analysis.....39

Table 3: New LA-ICP-MS trace element data (ppm) for Paniri samples obtained from nano-pellet analysis.....40

Table 4: New and published MC-ICP-MS whole-rock radiogenic isotopes data of selected samples from Toconce, as well as published radiogenic isotopes data of selected samples from Paniri.....42

Table 5: New and published laser fluorination O-isotope data for olivine, clinopyroxene and plagioclase crystals from selected eruptive units at Paniri and Toconce. $\delta^{18}O$ data reported in ‰ relative to the V-SMOW scale. Estimations of melt $\delta^{18}O$ values (i.e., $\delta^{18}O_{melt\text{-}ol}$, $\delta^{18}O_{melt\text{-}cpx}$, and $\delta^{18}O_{melt\text{-}plag}$) and calculated using an equilibrium mineral-melt fractionation factor of 1.3‰ for olivine and 0.7‰ for pyroxene (Bindeman et al., 2004) and 0.3‰ for plagioclase (Feeley and Sharp, 1995).....44

Table 6: New $\delta^{11}B$ (‰) data for Paniri and Toconce 45

List of Figures

Figure 1. schematic diagram of B cycle in subduction zones with approximate B concentrations and isotopic compositions of various reservoirs, taken from De Hoog and Savov (2018).....12

Figure 2. Schematic map showing the location of the separate volcanic segments of the Andes (Taken from González-Maurel, 2020).....15

Figure 3. 3-D representation of the 2.9 km/s velocity contour showing the distribution of the APMB and the location of representative Pliocene to Quaternary volcanoes erupted above the partial melt anomaly, modified from González-Maurel et al. (2019b, see Figure 11).....19

Figure 4. Google Earth™ satellite image of volcanoes forming the SPLVC. The dotted red triangles represent the geographical location of volcanic centres along the SPLVC, the stars represent the geographical location of Paniri (pink) and Toconce (orange).....20

Figure 5. (a) $^{143}Nd/^{144}Nd$ vs SiO_2 diagrams and (b) $^{87}Sr/^{86}Sr$ vs SiO_2 diagrams for samples with isotopic analyses of San Pedro-Linzor volcanic chain, taken from Godoy et al. (2014).....22

Figure 6. Study area showing the location of samples with isotopic values. The inset shows $^{87}Sr/^{86}Sr$ variations of the samples with the volcano location. White points represent volcanoes and black points represent dacitic domes. Taken from Godoy et al. (2014).....23

Figure 7. Sr concentrations show a decrease with increasing SiO_2 content of the samples. Figure modified from Godoy et al., 2014.....24

Figure 8. Paniri geological map taken from Godoy et al. (2018), see Figure 3.....25

Figure 9. Geological map of Toconce.....29

Figure 10. UCT δ11B vs GeoREM δ11B plot of geological reference material with known values from GeoReM database.....35

Figure 11. Total-Alkali vs. Silica (TAS) diagram for sampled lavas from Paniri and Toconce plotted with volcanoes from the San Pedro-Linzor Chain (after Godoy et al. (2014), coloured fields). The samples show well-defined

sub-alkaline trends, varying from andesitic to dacitic at Paniri, and basaltic-andesite to andesite at Toconce, in composition.....38

Figure 12. a) REE normalized to chondritic values (after Sun and McDonough, 1989) for representative lava samples at Paniri(black) and Toconce (red). The dark and light grey areas represent normalized composition of lavas erupted in the Central Andes (after (Mamani et al., 2010 and Godoy et al., 2019)). b) Trace elements normalized to primitive mantle diagrams (after Sun & McDonough, 1989) for Paniri(black) and Toconce (red), Gray area represents normalized composition of lavas erupted in the Central Andes (after (Mamani et al., 2010).....41

Figure 13. $^{87}Sr/^{86}Sr$ vs Sr (ppm) plot for analysed samples from Paniri, Toconce and the SPLVC (after Godoy et al., 2018). The curve represents the AFC model produced by Godoy et al. (2017). The white arrow represents a proposed trend for closed system fractional crystallization starting from a magma that was initially formed by an AFC process. Values along curve indicate the estimated melt fraction remaining from parent magma.....46

Figure 14. Binary mixing models of $\delta^{18}O$ estimated melt values from plagioclase, clinopyroxene, and olivine (in this work) versus (a) whole-rock SiO_2 and (b) $^{87}Sr/^{86}Sr$ ratios (from this work, Godoy et al., 2018, and González-Maurel et al., 2019). The Rayleigh fractionation trend illustrates the variation in $\delta^{18}O$ values expected from closed-system fractional crystallisation. The model indicates contamination of a starting sub-arc Andean parental magmas (S) by upper Central Andean continental crust considering two crustal compositions: C1 (after Damm et al., 1990) and C2 (after Davidson et al., 1990) (Table 2; after González-Maurel et al., 2020). 48

Figure 15. $\delta^{11}B$ values vs B-concentrations of investigated volcanic centres in the Central Andes from Schmitt et al., (2002), Rosner et al., (2003 Jones et al. (2014) and Godoy et al., (2023), uncertainty within symbol size...51

Figure 16. (A) B vs Nb (ppm), (B) B vs Nb/B, (C) δ11B vs Nb/B, and (D) δ11B vs B of Paniri and Toconce plotted in context of investigated volcanic centres in the Central Andes from Schmitt et al., (2002), Rosner et al., (2003), Jones et al. (2014) and Godoy et al., (2023).....53

Figure 17. $\delta^{11}B$ vs $^{87}Sr/^{86}Sr$ plot showing crustal influence on δ11B values at Paniri and Toconce.....56

Figure 18. Distribution of samples from the same eruptive unit taken at Toconce.....57

Figure 19. $\delta^{11}B$ vs $^{87}Sr/^{86}Sr$ at Toconce showing Intra- and Inter-unit variations.....58

Figure 20. After Godoy et al. (2023) modified modelling from Rosner et al., 2003. (a) B-Sr static and (b) B-Sr dynamic mixing model. Rosner et al. (2003) data plotted as gray circles, and Godoy et al. (2023) La Poruña data plotted as yellow stars, Paniri plotted as pink diamonds and Toconce plotted as orange triangles). In the static mixing model, there is no slab-fluid isotopic fractionation occurring, yielding a subduction-modified parental arc melt with a $\delta^{11}B$ value of +5.1 ‰. In the dynamic mixing model, the $\delta^{11}B$ value of the slab-derived fluid changes as a function of distance from trench, yielding a subduction-modified parental arc melt with $\delta^{11}B$ values between -2.8 ‰ (for addition of back arc fluids; BA) and +6.4 ‰ (for addition of volcanic front fluids; VF). The solid black arrow-lines represent an isotopic composition of primary arc magmas produced by mixing between the mantle wedge and end-member fluids derived from the subducting slab. The model involves two steps, (1) a primary mantle-like derived melt is mixed with no more than 2% of an AOC-derived slab fluid (mixing curves shown after Rosner et al., 2003). This yields a subduction-modified parental arc melt with $\delta^{11}B$ value between -2.8 ‰ (for addition of back arc fluids; BA) and +6.4 ‰ (for addition

of volcanic front fluids; VF). (2) Mixing of the modified parental melt with Andean crust (Godoy et al., 2023).....60

Figure 21. $\delta^{11}B$ vs $^{87}Sr/^{86}Sr$ plot showing crustal influence on δ11B values between two relatively older (i.e., Paniri and Toconce) and two relatively younger (i.e., La Poruña (Godoy et al., 2023), and San Pedro (unpublished)) volcanic centres along the SPLVC.....62

1. Introduction

1.1. Arc Magmatism

Subduction is a tectonic process that results from the movement of tectonic plates relative to one another, and it is a fundamental and very important geological process on the earth (Stern, 2002). This process recycles the old oceanic and continental crust at convergent plate boundaries, linking the earth's surface to its interior. This process is countered by spreading (or divergence) as observed at Mid-Oceanic Ridges (MOR) (Elburg, 2010; Marschall, 2018). Subduction-related magmatism occurs at active margins where older and/or denser oceanic lithosphere, containing abundant water, subducts beneath another tectonic plate. It occurs in two main settings: (i) ocean-ocean plate boundaries (i.e., island arcs, e.g., Sunda, Java, Japan, etc) and (ii) ocean-continental plate boundaries (i.e., continental arcs, e.g., Andes, Alaska, Kamchatka, etc). The subducting oceanic lithosphere is warmed by frictional heating on the fault plane between downward moving oceanic lithosphere and the overlying mantle wedge. This leads to prograde dehydration reactions on the subducting slab, releasing slab components (i.e., aqueous fluid, hydrous partial melts, or supercritical fluids) from hydrous minerals (e.g., mica, amphibole, serpentine, chlorite, etc.; Tatsumi et al., 1986) and thus carrying fluid-soluble elements from the subducting oceanic lithosphere into the overlying mantle wedge. The addition of components from the subducting slab into the mantle wedge plays an important role in the generation of magmas in subduction zones.

Components released from the subducting slab lead to the generation of molten magma at slightly lower temperatures (than the normal melting adiabatic curve) in the overlying mantle wedge, through a process of partial melting. This molten magma is less dense than the surrounding mantle and therefore rises through the overlying crust. The release of volatiles also influences the geochemical composition of the sub-arc mantle (Murphy, 2006; Elburg, 2010). This dehydration then initiates a chain of events, that together build-up to the generation of magma that rise to form volcanic arcs (Murphy, 2006). Continental arc magmatism differs from island arc magmatism mainly in that volcanoes in continental arcs sit upon

continental crust, which is much thicker compared to the oceanic crust in island arcs. The thickness and low density of the continental crust may also slow down the rate of magma ascent, resulting in the stagnation of parental mantle-derived magmas and a greater potential for magma-crust interaction, crustal contamination, and further differentiation. Since parental mantle-derived magmas must pass through a very thick continental crust, mafic material is extremely rare in continental arcs, such as the Andes of South America, making the information about the mantle difficult to constrain or explore.

The Andes building process witnessed today is of much importance as it presents a modern example of oceanic-continental convergence. This further provides a modern-day analogue that can be used to interpret older converging mountain belts around the world. The Andes are formed as a result of the eastward moving Nazca and Antarctic oceanic plates subducting under the South American continental plate. Magmatism in the Andes has been associated with the dehydration and/or melting of the subducting oceanic lithosphere and a subsequent interaction of these slab-derived components with the overlying mantle wedge (Stern, 2004; Goss and Kay, 2009). Slab-derived components are very complex and not easy to study because they are highly heterogeneous due to their interaction with many components (e.g., lithospheric mantle, sediments, hydrothermal fluids, lower and upper crust, etc.) from the time of their formation until time of eruption (if they erupt) (González-Maurel et al., 2019a, 2020).

Geochemical studies have identified and established boron concentrations and boron isotopes as sensitive indicators of subducting slab components in arc magmatic rocks (e.g., Palmer, 1991; Rosner et al., 2003; Tonarini et al., 2011; Jones et al., 2014 etc). Boron is a good example of a fluid mobile element that can be used to trace the hydration of the overlying mantle wedge in subduction zones (Hemming and Hanson, 1992; Barth, 1998; Peacock and Hervig, 1999; Marschall and Schumacher, 2012; Marschall, 2018). The boron isotope composition, expressed with the standard notation $\delta^{11}B = ((^{11}B/^{10}B(sample)/^{11}B/^{10}B(reference))-1) \times 1000$, is useful in detecting and quantifying the exchange process between the slab and the mantle (Marschall, 2018; Marschall and Foster, 2018).

1.2. Boron isotopes in volcanic arc settings

Arc magmas are distinguished from other magmatic settings (e.g. at divergent boundaries, intraplate, and collision related convergent boundaries) mainly because of: (i) the presence of volatiles/fluids that are released from the subducting oceanic lithosphere, (ii) the different geothermal regimes that exist at destructive plate margins and (iii) the compressive tectonic setting that inhibits the upward movement of magma, therefore allowing for an extensive interaction between the rising magma and the adjacent wall rock (Murphy, 2006, Elburg, 2010).

Boron (B) is a chemical element with a low atomic mass with two stable isotopes ^{10}B and ^{11}B, at approximately ~20% and ~80% abundances respectively. B is very useful as geochemical tracer of mass transfer at subduction zone settings because of its high mobility during high- and low-temperature fluid related processes. Boron shows a strong affinity for silicate melts and aqueous fluids. Low temperature altered oceanic basalts, ocean sediments and serpentines are characterised by very high B abundances (10-200 µg/g) and the mantle derived material is characterised by very low B abundances (<0.1 µg/g), see Figure 1 (Leeman and Sisson, 1996; Marschall, 2018).

According to Peacock and Hervig (1999), the principle behind B isotope fractionation is that fractionation occurs as a result of the difference in B coordination from trigonal boron in neutral pH hydrous fluid to a tetragonally coordinated boron in many rock forming minerals (Marschall and Foster, 2018). Experimental studies of isotopic fractionation of boron between hydrous fluids, melts, and minerals have indicated that ^{11}B prefers to enter the fluid relative to the melt or mineral. The fractionation properties of the two stable isotopes, ^{10}B and ^{11}B, at low temperatures is largely responsible for surface reservoirs that are enriched in $\delta^{11}B$, and thus B-isotope systems have been widely used for studies on processes acting on the earth's surface (e.g., Hemming and Hanson, 1992; Barth, 1998; Marschall, 2018; Marschall and Foster, 2018). Marschall (2018), and Marschall and Foster (2018) reviewed data from some important studies on B-isotopes as observed in MORB and OIB, and they concluded that the B-isotopic composition of pristine, uncontaminated MORB has been determined as $\delta^{11}B = -7.1\pm0.9‰$ whilst that of oceans/sea water is $\delta^{11}B = +39.6‰$ (Figure 1). Variations, if there are any, of the $\delta^{11}B$ in OIB magmas tend to

be approximately 4% higher than or 5% lower than the MORB $\delta^{11}B$ value (i.e. -10±2 to -4±1‰) (Marschall, 2018).

Prior to entering the subduction zone, the subducting oceanic crust and sediments have been modified by their interaction with the hydrosphere. These are all eventually subducted at convergent plate margins, introducing chemical and isotopic differences into the mantle wedge (Marschall and Schumacher, 2012; Marschall, 2018). Boron is an ideal geochemical tracer that is used to detect and quantify the exchange processes between the subducting slab and the mantle (Marschall, 2018, Marschall and Foster, 2018). Boron isotopes show great differences between the mantle ($\delta^{11}B$ = -7.1‰), crust ($\delta^{11}B$ = +2 to +26 ‰), and hydrosphere ($\delta^{11}B$ = -9 to +16 ‰) (Marschall, 2018). Therefore, any assimilated seawater influenced materials or altered oceanic crust into magmas lead to elevated $\delta^{11}B$ values.

The B elemental concentrations, similarly, are low for material derived from the mantle (1 to 80 ppm) and high for sediments (+2 to +26 ppm) and altered oceanic crust (0 to 18 ppm) (Marschall and Foster, 2018). The significant compositional difference between the continental crust, modern sea water and the depleted mantle makes boron a good tracer for the evolution of the ocean-crust-mantle system (Marschall and Foster, 2018).

Studies on arc related magmas, generally agree that at subduction zone settings, melting is initiated in the asthenospheric mantle wedge above the subducted oceanic lithosphere. This is due to the mantle wedge solidus temperatures being reduced by the influx of H_2O-rich fluids/melts that are released from the subducted oceanic lithosphere (Gill, 1981; Tatsumi et al., 1986; Tatsumi and Eggins, 1995; Rosner et al., 2003; Grove et al., 2012). These volatiles are responsible for transporting fluid-mobile elements into the mantle wedge, and thus thought to be responsible for the "subduction component" that distinguishes most arc magmas from MORB and other mantle-derived magmas (Rosner et al., 2003).

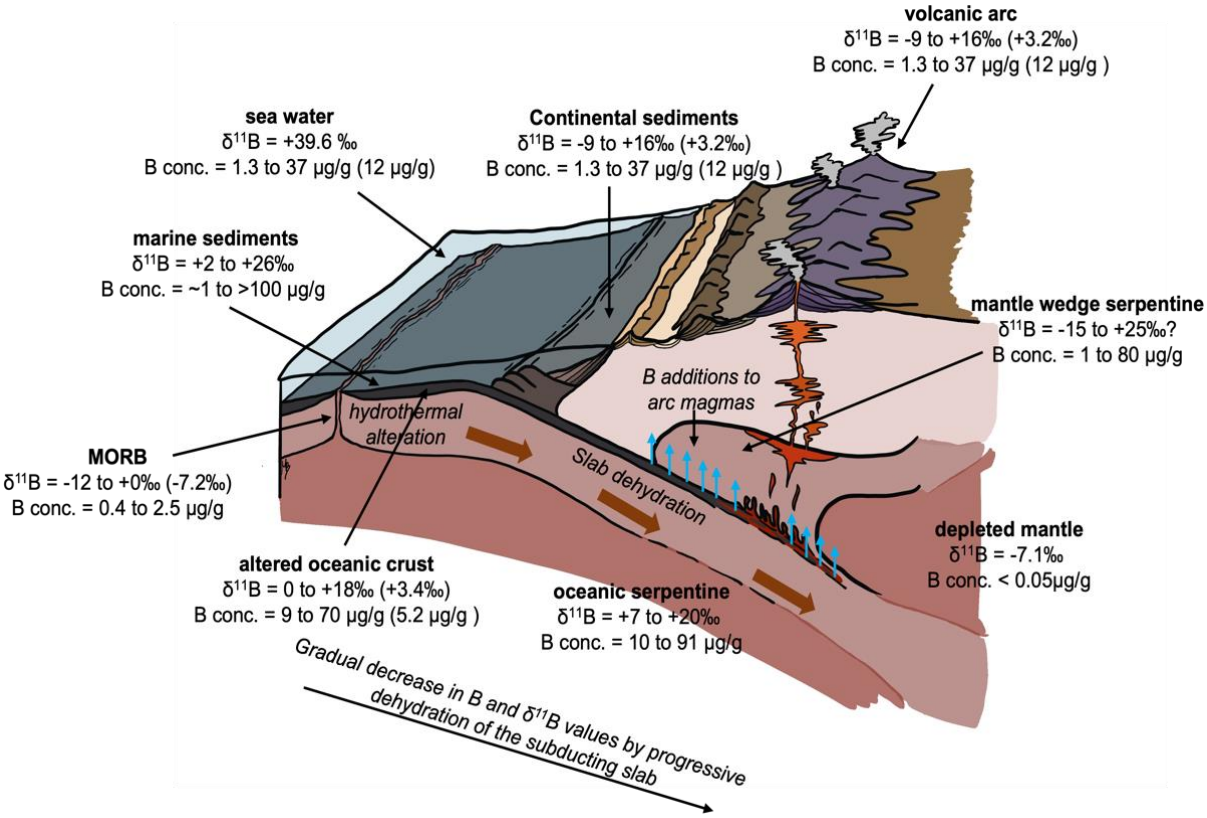

Figure 1. schematic diagram of B cycle in subduction zones with approximate B concentrations and isotopic compositions of various reservoirs, taken from De Hoog and Savov (2018).

1.3. Objectives/aims of study:

Very little work has been done on boron (B concentrations and B isotopes $\delta^{11}B$) in the Andes especially with respect to whole rock $\delta^{11}B$ geochemistry (e.g., Kasemann et al., 2000; Schmitt et al., 2001; Rosner et al., 2003; Wittenbrink et al., 2009; Jones et al., 2014 and Godoy et al., 2023). The published studies (exept Godoy et al., 2003) focused primarily on the upper continental crust and comparisons between the B variations within the Central Andes. $\delta^{11}B$ characteristics of parental melts have not been studied in detail for the different eruptive units in individual volcanoes. This includes the boron isotope variations between different eruptive units and the boron isotope variations within each eruptive unit. This may provide new information about the influence, and temporal change, of slab-derived fluids and magma contamination on boron isotope signatures.

To better understand such behaviour/systematics of boron isotopes, Paniri (22°03’34”S, 68°13’42”W; Figure 4) and Toconce

(22°11’17’’S, 68°04’43’’W; Figure 4) volcanoes which are relatively older than neighbouring volcanoes in the Chilean Altiplano were selected, and they form part of the San Pedro-Linzor Volcanic Chain (extending between 21°53’S 68°23’W and 22°09’S 67°58’W; Figure 4). The Paniri-Toconce volcanic chain is made up of an aligned structure oriented at NW-SE corresponding to the San Pedro-Linzor Volcanic Chain (SPLVC), and this volcanic chain is distinguished by a strong structural control at the time of its evolution (Polanco et al., 2012).

New boron elemental and isotopic data for several well-characterised lava samples from both Paniri and Toconce are presented in this manuscript. Boron isotope analyses were made (i) within units of each volcano, (ii) between the two volcanoes, (iii) with regional B isotope data and (iv) with B isotope data from arc systems globally. This study will therefore contribute to our understanding of the role of subduction-related components to mantle melting and magma-crustal interactions at these various scales.

2. Geological context

2.1. Regional geological context

2.1.1. The Andean Cordillera

The Andes Cordillera forms the longest continental mountain chain (>7500 km) globally and is located along the western margin of South America (Figure 2), stretching from the Caribbean Coast (north) to Cape Horn (south) (Wörner et al., 1988; Stern, 2004). In the Andes, the generation of magma is associated with the subduction of the Nazca and Antarctic lithosphere beneath the South American plate. According to Stern (2004), there are over two hundred potentially active Quaternary volcanoes and at least twelve larger caldera/ignimbrite systems in this magmatic arc. The Andes active volcanism occurs in areas where there is a relatively steep angle of subduction (>25°), and the active arc segments are separated by regions below which the subduction angle decreases and becomes relatively flat (<10°) at depth approximately >100 km (Beck et al., 1996; Stern, 2004). Parts of the low angle subduction in the Andean Cordillera formed at the beginning of the Miocene in association with the low angle subduction of buoyant oceanic plateaus (de Silva, 1989; Beck et al., 1996; Stern, 2004). At present, the segmentation geometry and active Andean volcanic zones are clearly short-lived features related to the Neogene tectonics (Stern, 2004).

The volcanic structures of the Andean Cordillera occur in four separate segments or Volcanic Zones (VZ) referred to as the (i) Northern (NVZ; 12°N-05°S), Central (CVZ; 05°-33°S), Southern (SVZ; 33°-56°S), and the Austral (AVZ; 49°N-55°S) Volcanic Zones, all separated by zones of volcanic inactivity (Figure 2).

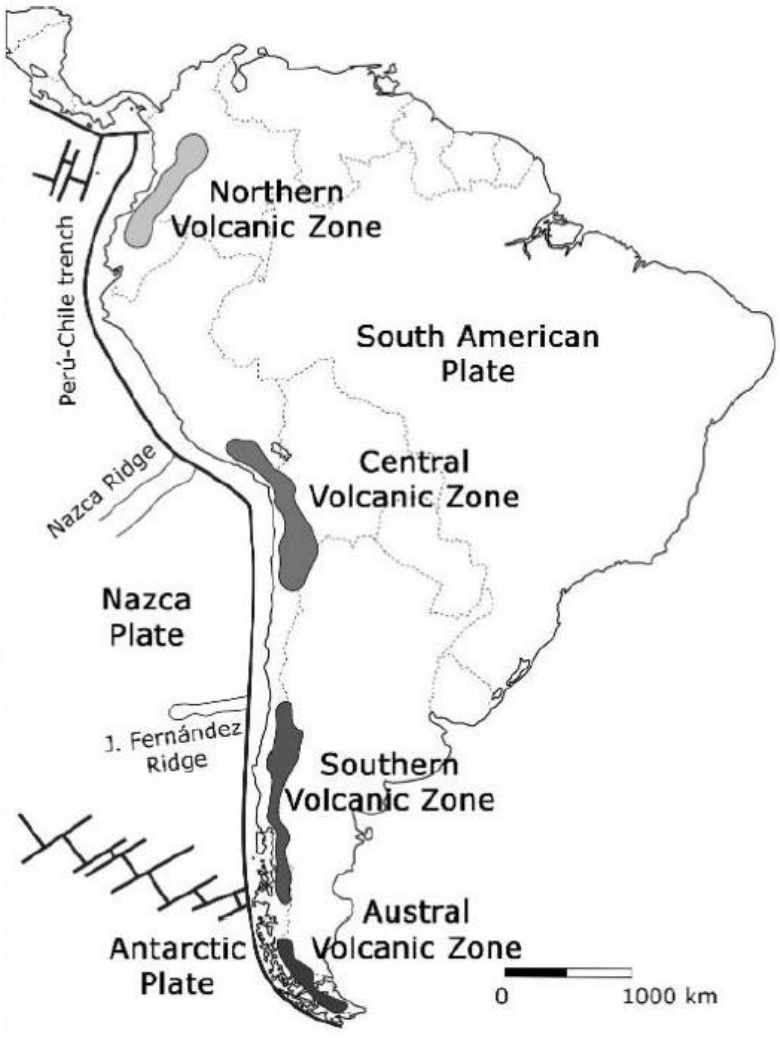

Figure 2. Schematic map showing the location of the separate volcanic segments of the Andes (Taken from González-Maurel, 2020).

2.1.2. Central Volcanic Zone

The Central Volcanic Zone (CVZ) is a volcanic arc segment located on the western margin of South America extending from latitude of 14°S to 27°S (Figure 2) (de Silva, 1989; Davidson et al., 1990; Godoy et al., 2014, 2018). It includes southern Peru, northern Chile, adjacent parts of Bolivia, and Argentina. The evolution of the CVZ involved an eastward migration of associated volcanic fronts, and this migration is attributed to: (i) subduction of the Nazca plate below the South American plate since the Jurassic and the changes in the angle of subduction over the last 200 Ma, and (ii) subduction erosion that affected

the leading edge of the upper plate in this zone (de Silva, 1989; Stern, 1991; Godoy et al., 2014, 2018).

At present day, the Eocene crust being subducted below the South American continental margin is ~50 Ma (Rosner et al, 2003). The CVZ has been a key focus of many isotopic and petrological studies, often referenced as an important example of subduction related volcanism at a continental margin (Grunder, 1987). The continental crust in the CVZ is about 70-74 km thick at maximum thickness (the thickest crust in any subduction zone on earth), with a felsic upper crust and mafic lower crust that has varying thicknesses (~20 to 30 km) (James, 1971, Beck et al., 1996). In the CVZ, volcanic rocks have chemical and isotopic signatures that argue for significant crustal interaction during the time of their formation (Grunder, 1987; Trumbull et al., 1999; Godoy et al., 2014; González-Maurel et al., 2019a, 2019b).

The CVZ together with the NVZ and SVZ, are recognised as the three most active volcanic zones along the Andean magmatic arc (de Silva, 1989; Davidson et al., 1990). The magmatic activity in the CVZ is heavily influenced by processes of differentiation and assimilation that occurred at regions of high and low pressure beneath the thick continental crust (Godoy et al, 2014; González-Maurel et al., 2019a). The composition of dominating eruptions in the CVZ is mostly andesitic to dacitic lava flows and regionally voluminous dacitic to rhyolitic ignimbrites associated with the Altiplano-Puna volcanic complex (de Silva and Francis, 1989, Wörner et al., 2000; Stern, 2004; Godoy et al., 2014).

Godoy et al. (2014) suggested that the process of subduction cannot fully explain all the isotopic signatures of magmatism in the Central Andes. This is mainly because the magma generating processes that occur at the lower levels of a thick continental crust (such as in subduction zone settings) are strongly influenced by differentiation and assimilation at high pressure conditions. This is typically represented or shown by high light to heavy rare earth element ratios (LREE/HREE) of the erupted lavas. An increase of this ratio is understood as indicating a change to magma evolution in the presence of garnet during evolution of the Central Andes (Mamani et al., 2010, Godoy et al., 2014). The geochemical signals could be introduced into magmas as high-pressure fractionation with garnet on the liquidus and/or residual garnet. It is suggested that because

we do not observe garnet trace element signatures in all magmas, which would suggest high pressure magma sources, subduction cannot be the only cause of magmatism in this area (Godoy et al., 2014). The combination of both the subduction of oceanic crust into sub-arc mantle and the assimilation of continental crust into mantle derived magmas are means by which the continental crust is incorporated into mantle derived Andean magmas (Stern, 2004, González-Maurel et al., 2019a,b).

2.1.3. Altiplano-Puna Volcanic Complex

The Altiplano-Puna volcanic complex (APVC) is a major volcano-tectonic complex that developed at the Altiplano and Puna plateaus (21°-24°S), as a result of a late Miocene silica-rich (>65% wt.) ignimbrite flare-up of high volume (de Silva, 1989, Chmielowski and Zandt, 1999). The APVC complex covers an area of >70 000 km², with the dominant elements of the ~50 000 km² complex stretching from the southwards transition between Altiplano (~4000 m a.s.l.) and Puna (~5000 m a.s.l.) plateaus. It sits at approximately 100-250 km above the Nazca plate and accounts for the largest ignimbrite concentration in the CVZ with a 15 000 m^3 magnitude (de Silva, 1989; Chmielowski and Zandt, 1999). According to de Silva (1989), effusive andesitic volcanism dominated throughout the APVC from early to late Miocene. Voluminous and extensive ignimbrite eruptions took over from the late Miocene to early Pleistocene (de Silva et al., 1989 and 1994; Schmitt et al., 2001; Lindsay et al., 2001; de Silva et al., 2006).

The timing of crustal thickening in the CVZ coincides with the sudden eruption of ignimbrites in the APVC (Isacks, 1988; de Silva, 1989), which further coincides with the rapid subduction along the Andean margin, influencing the amount of heat addition to the crust through the intrusion of mafic magmas. Several studies (e.g., de Silva, 1989; de Silva and Francis, 1989; Wörner et al., 2000; Stern, 2004) suggested that; 1. the primary cause of the flare-up and other evolved volcanic products is crustal melting. The crustal melting is believed to have been caused by the crustal thickening that is associated with the construction of the central Andes magmatic arc. 2. this would mean that subduction related melting contributes lesser melt in the APVC (de Silva, 1989). Davidson et al. (1990) and Mamani et al. (2010)

interpret these magmas as being derived from the mantle wedge and modified by 20-40% of crustal assimilation.

Studies by e.g., Chmielowski et al. (1999), Zandt et al. (2003) and Ward et al. (2014) argued for an area of regional magma generation and storage below the APVC. Through geophysical methods, Chmielowski et al. (1999) proposed a very low-velocity layer at depths of ~19 km below the APVC, with Vs <0.5 km/s and a thickness of 750-810 m. Zandt et al. (2003) approximated this layer to stretch to an area of ~60 000 m^2. These characteristics were consistent with a sill-like magma body, and they suggested that this magma body is associated with the APVC volcanoes (Zandt et al., 2003). This low-velocity zone (LVZ) sill-like magma body is called the Altiplano-Puna Magma Body (APMB) (Chmielowski et al., 1999).

2.1.4. Altiplano-Puna Magmatic Body

The Altiplano-Puna Magma Body (APMB) is a magma body (Figure 3) located within the Altiplano-Puna plateau, ~10-20 km below the APVC, central Andes (Chmielowski et al., 1999). The APMB underlies much of the APVC and is a zone characterised by geophysical features such as low seismic velocities (low Vs, at depths 10-20 km), extremely high electrical conductivity (at depths 10-30 km) and thermal anomalies (Chmielowski et al., 1999; Zandt et al., 2003). It extends from 4 km to 30 km below the crustal surface with partially molten material having a diameter of ~200 km, thickness of ~11 km and a volume of approximately ~500 000 km^3 (Zandt et al., 2003; Ward et al., 2014).

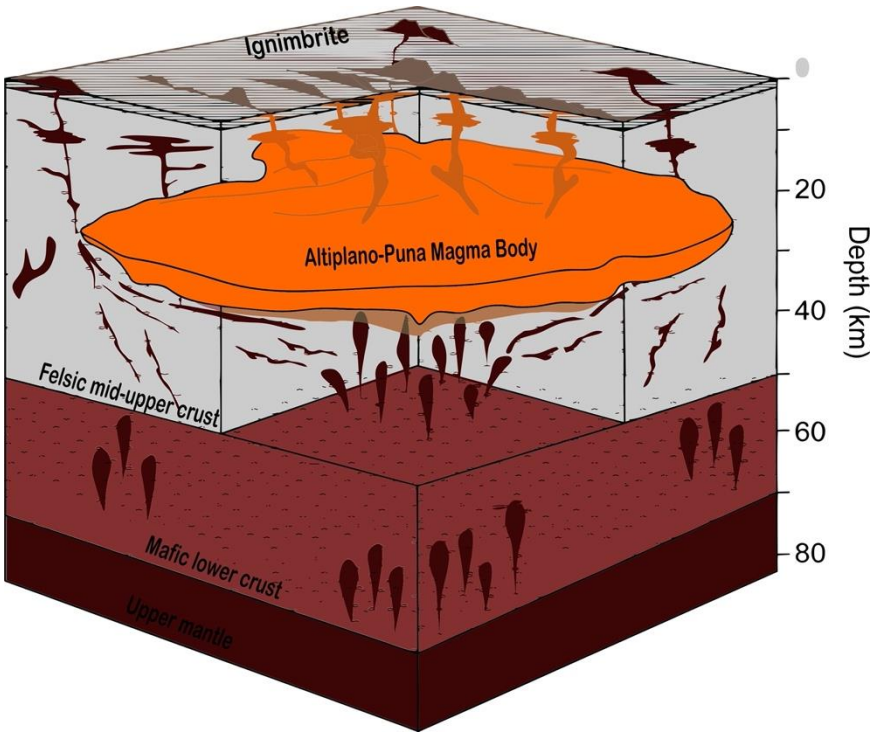

Figure 3. 3-D representation of the 2.9 km/s velocity contour showing the distribution of the APMB and the location of representative Pliocene to Quaternary volcanoes erupted above the partial melt anomaly, modified from González-Maurel et al. (2019b, see Figure 11).

Zandt et al. (2003) and Ward et al. (2014) suggested that the APMB holds ~4% partial melt in a melt-crystal mush state in zones with S-velocities of 3.2 km/s, to ~10% (2.9 km/s), and up to ~25% (<1.9 km/s). This partial melt is related to the crustal deformation linked to magma rising beneath the APVC.

Godoy et al. (2017) and González-Maurel et al.(2019b) proposed lateral compositional variations of magmas that are erupted across the margins of the APMB. Ascending mafic magmas interact with the APMB to different degrees, with more differentiation increasingly evident from the edge/border towards the centre.

2.2. Local geological context

2.2.1. San Pedro-Linzor Volcanic Chain (SPLVC)

The San Pedro-Linzor volcanic chain (SPLVC) is a NW-SE trending lineament of volcanic structures, extending between 21°53’S 68°23’W and 22°09’S 67°58’W, in the Central Andes of Northern Chile (Figure 4). Available ages suggest that the evolution of

this volcanic chain falls in the Pleistocene (Stern, 2004; Stern et al., 2007). According to Godoy et al., (2017), the SPLVC evolved over the last 2 Ma during a waning of the ignimbrite flare-up in the APVC. This volcanic chain is ~65 km long and situated along the western margin of the APMB and north-western border of the Altiplano-Puna Volcanic Complex on top of an exceptionally thick (~70 km) continental crust (de Silva, 1989; Beck et al., 1996; Yuan et al., 2002; Godoy et al., 2014, 2020). The SPLVC in its orientation is distinct with respect to the N-S orientation of the Central Volcanic front (active volcanism) in northern Chile. Its orientation parallels the Lípez-Coranzuli, Pastos-Grandes and Calama-Olacapato-El Toro fault systems, which are the two major regional lineaments of Paleozoic age (Godoy et al., 2014).

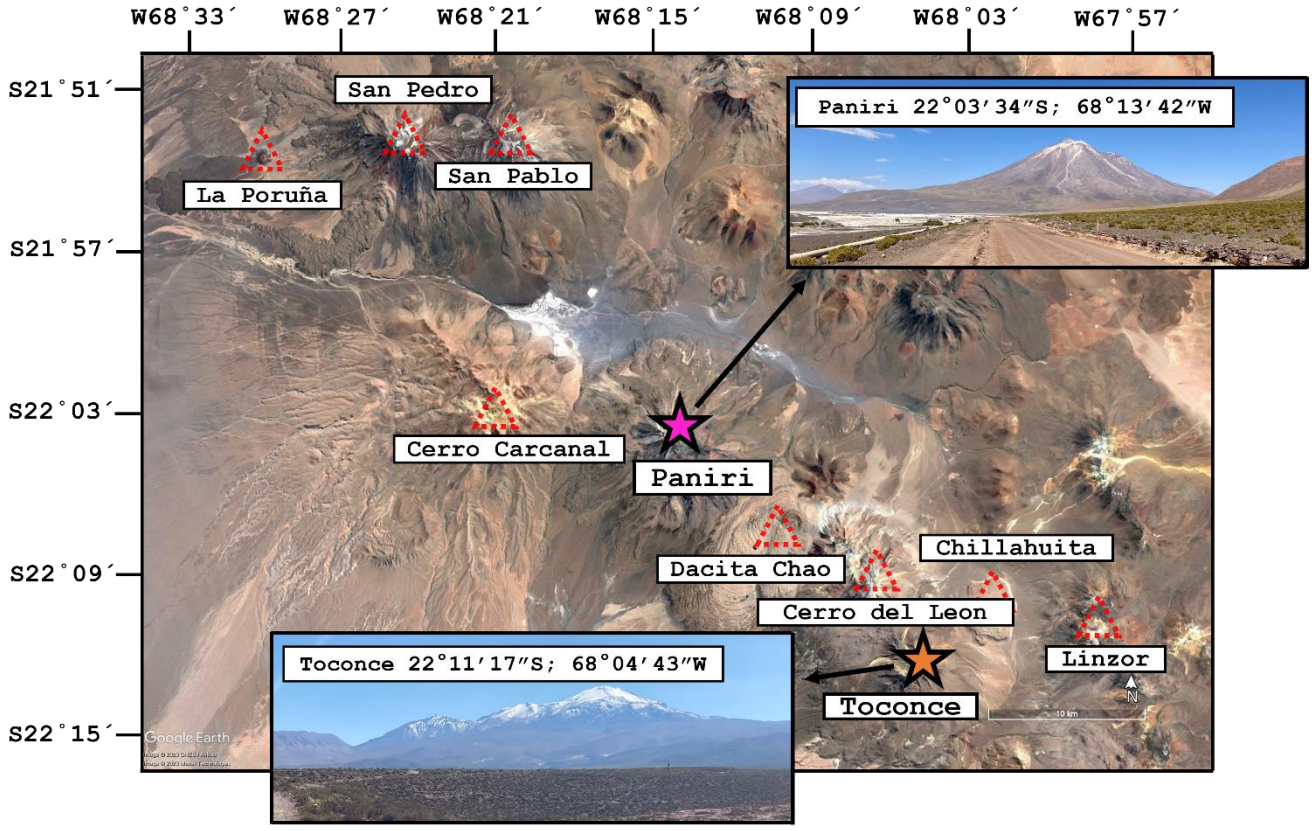

Figure 4. Google Earth™ satellite image of volcanoes forming the SPLVC. The dotted red triangles represent the geographical location of volcanic centres along the SPLVC, the stars represent the geographical location of Paniri (pink) and Toconce (orange).

The basement of the very thick continental crust below the SPLVC is constituted of felsic, Proterozoic upper crust, and a thin mafic lower crustal section (<25 km) (Stern, 2004; Godoy et al.,

2014). The SPLVC is composed of a series of large and complex volcanic products (e.g., lava flows and scoria fragments) that form mainly scoria cones (e.g., La Poruña), stratovolcanoes (e.g., San Pedro, Paniri, and Toconce), and coulee flows that consist of lavas, pyroclastic and scoria flows and breccias (Godoy et al., 2017, 2020). The complex volcanic centres that make up the SPLVC are, San Pedro; San Pablo; Paniri; Cerro del Leon; Toconce; and Linzor. Petrographically the lava flows making up the SPLVC vary from basaltic-andesite, hornblende-dacite, dacitic pyroclastic flows, dacitic pyroclastic flows, and basaltic-andesite to andesitic flows (Godoy et al., 2014; see Fig. 3).

Geochemical and isotopic data suggest that, during the evolution of the SPLVC over the past 2 Ma, the upper crustal magmatic evolution of the SPLVC occurred in two stages of magma migration: the first being the interaction of primitive magmas with the APMB at 10-40 km crustal depth; and, the second being the stagnation of the parental magma of each individual volcanic structure (Godoy et al., 2014, 2017; González-Maurel et al., 2019b). The interaction of primitive magmas with partially molten domains (APMB) of the crust at depths of 10-40 km and the primitive magmas corresponding to mantle values have been recognised in the Central Andes (e.g., Davidson et al., 1990; González-Maurel et al., 2019a, 2020; Burns et al., 2020). These primary melts ascent through the thick crust via points of crustal weaknesses and stagnate at mid crustal levels (de Silva and Kay, 2018; Godoy et al., 2019; González-Maurel et al., 2019a). The underplating of the primary melts also thermally sustains the APMB (de Silva et al., 2006; González- Maurel et al., 2019b).

Radiogenic isotope ratios are used as ideal measures of crustal contamination in the Central Andes. Godoy et al. (2014) recorded $^{87}Sr/^{86}Sr$ and $^{143}Nd/^{144}Nd$ ratios of analysed lava flows from the San Pedro-Linzor chain, which vary between $^{87}Sr/^{86}Sr$ values of 0.7063-0.7094 and $^{143}Nd/^{144}Nd$ values of 0.5118-0.5124. When the $^{87}Sr/^{86}Sr$ values are compared to geochemical data of most lavas erupted in the Central Andes (<0.708 mainly basaltic andesite), they are found to be at the higher end of the range of $^{87}Sr/^{86}Sr$ values. The $^{143}Nd/^{144}Nd$ ratios on the other hand are found to be at the lower end of the range.

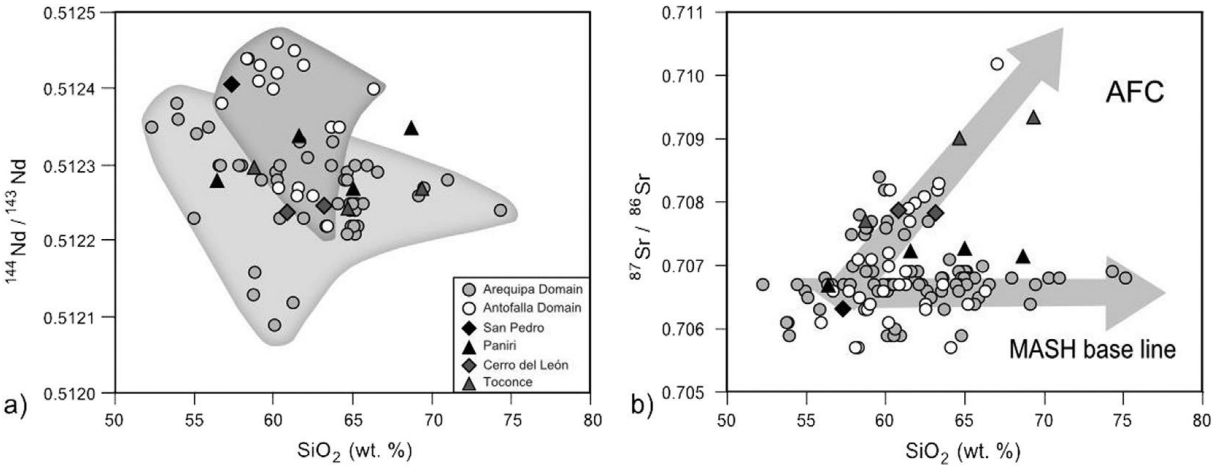

Figure 5. (a) $^{143}Nd/^{144}Nd$ vs SiO_2 diagrams and (b) $^{87}Sr/^{86}Sr$ vs SiO_2 diagrams for samples with isotopic analyses of San Pedro-Linzor volcanic chain, taken from Godoy et al. (2014).

The isotopic values recorded from the San Pedro-Linzor lava flows were compared with regional data (Figure 5) (Mamani et al., 2010). While the $^{143}Nd/^{144}Nd$ ratios do not show any correlation with fractionation (Figure 5a), the $^{87}Sr/^{86}Sr$ ratios reveal two distinct trends in the $^{87}Sr/^{86}Sr$ versus silica diagram (Figure 5b). A trend follows the MASH baseline at constant Sr isotope ratios with increasing SO_2 content. A second trend shows increasing $^{87}Sr/^{86}Sr$ ratios with increasing SiO_2, suggesting assimilation with fractional crystallisation (AFC). These two different magma evolution regimes were related to the development of the APMB in the last 10 Ma in the area (Godoy et al., 2014).

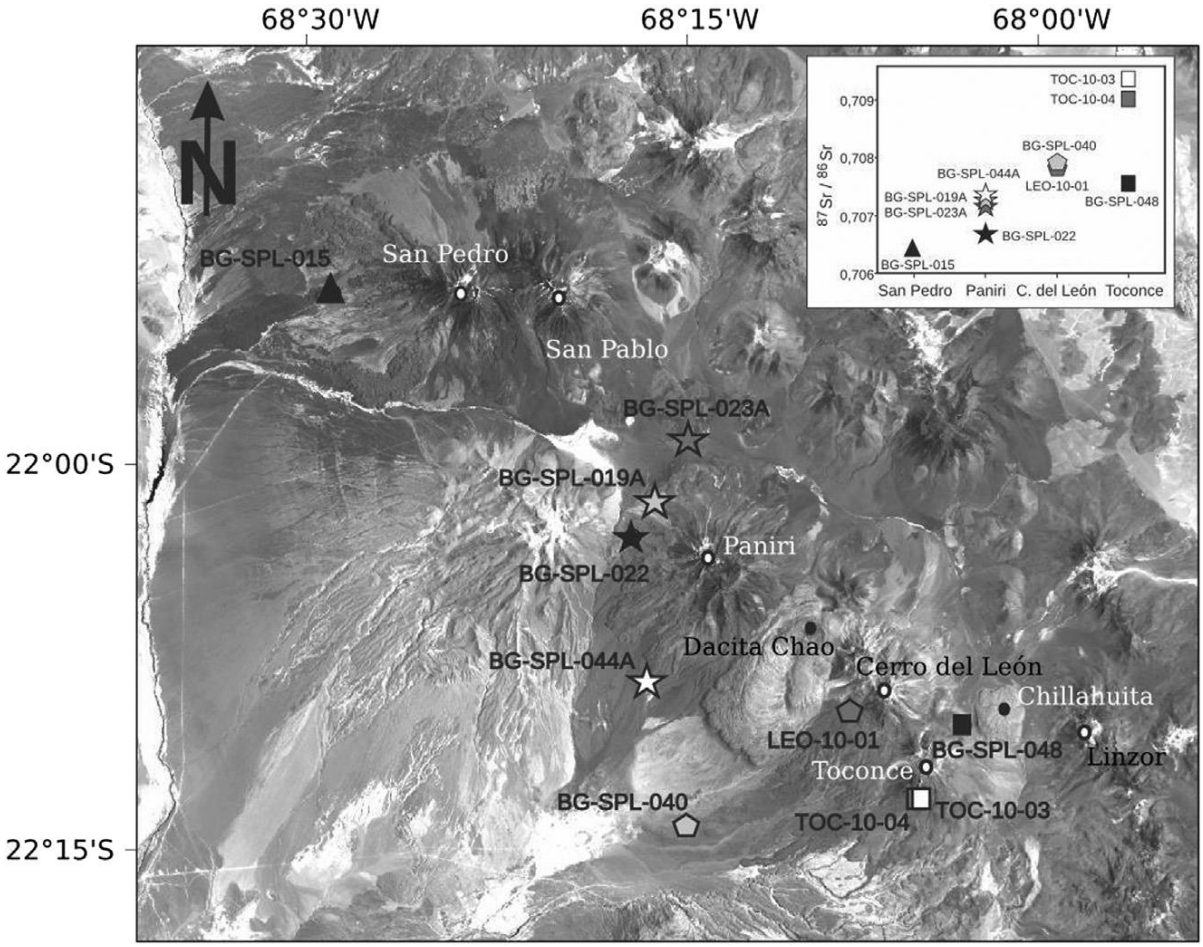

Figure 6. Study area showing the location of samples with isotopic values. The inset shows $^{87}Sr/^{86}Sr$ variations of the samples with the volcano location. White points represent volcanoes and black points represent dacitic domes. Taken from Godoy et al. (2014).

Figure 6 shows a NW to SE increase in $^{87}Sr/^{86}Sr$ ratios with increasing SiO_2 (wt.%) content of the lavas of the volcanic chain. Godoy et al. (2017) and González-Maurel et al. (2019a) observed that the Sr isotopic variations are explained by systematic, variable degrees of differentiation and contamination along the volcanic chain and related to the location of the APMB.

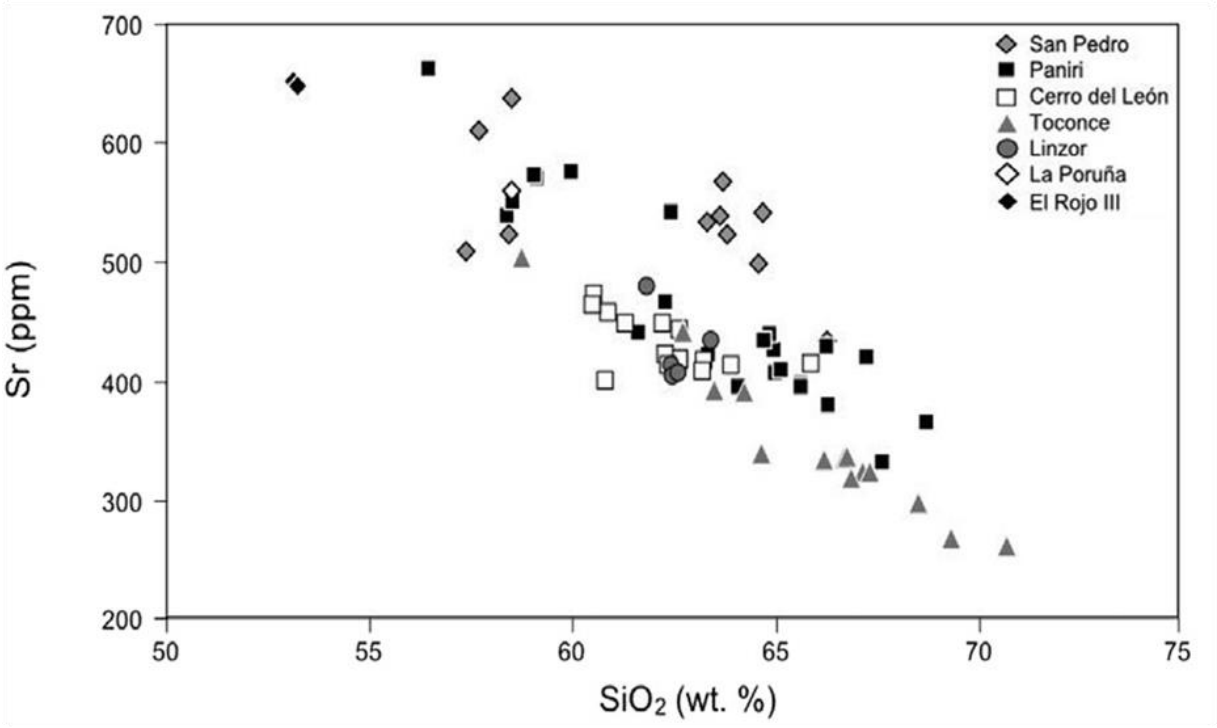

Figure 7. Sr concentrations show a decrease with increasing SiO_2 content of the samples. Figure modified from Godoy et al., 2014.

2.2.2. Paniri Volcano

Paniri volcano (Figure 8) is a Pleistocene age stratovolcano that is located at 22°03'34"S and 68°13'42"W, in the SPLVC (de Silva, 1989; Godoy et al., 2018). Paniri has an elevation of ~5 560 m and prominence (or summit) of ~1 653 m. It has three craters and there is no evidence of any recent eruptions, however the volcano has potentially been active in the past ten thousand years.

According to de Silva (1989), Paniri is potentially an active volcano, as suggested by presence of uneroded lavas, a small scoria cone on the extreme summit and a well-preserved summit crater.

z

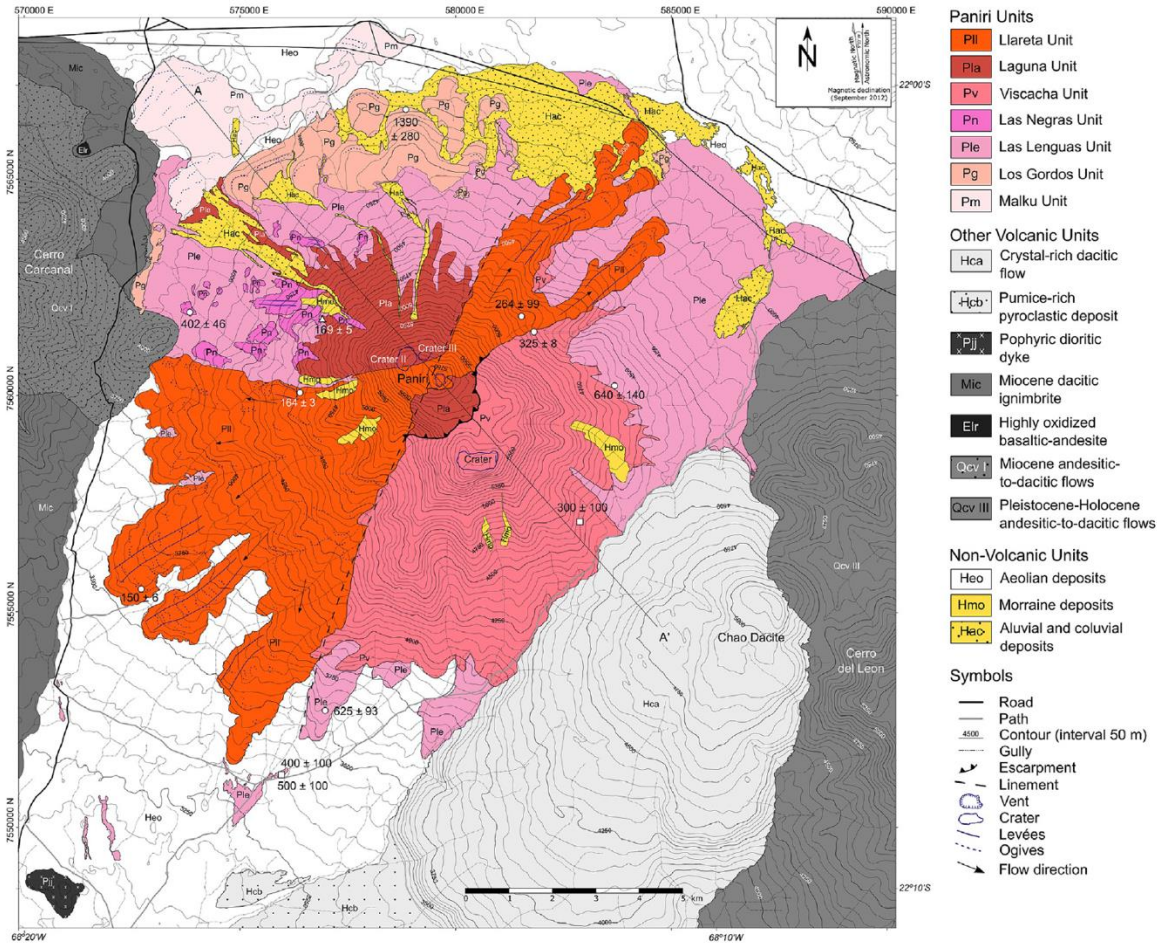

Figure 8. Paniri geological map taken from Godoy et al. (2018), see Figure 3.

Godoy et al. (2018) studied the volcanological evolution of Paniri, with a focus on the sequences of the main eruptive events of the volcano. Paniri sits on top of Miocene ignimbrite (rhyodacitic-to-rhyolitic) fields and an Oligocene-to-Lower Miocene volcano-sedimentary sequence outcropping further south. They identified seven different units that geochemically range from basaltic-andesite to rhyolite with a main calc-alkaline trend. These units are named: Malku, Los Gordos, Las Lenguas, Las Negras, Viscacha, Laguna, and Llareta (from oldest to youngest).

Seelenfreund et al. (2009) and Godoy et al. (2017, 2018) published $^{40}Ar/^{39}Ar$ and K/Ar ages for Paniri. The ages suggest seven different volcanic units were erupted during four main eruption phases which occurred over a period of more than 1 Myrs (Godoy et al., 2017; 2018). These eruption phases in

chronological order are (i) Plateau shield (>800 ka); (ii) Main edifice (800-400 ka); (iii) Old Cone (400-250 ka); and (iv) New Cone (250 ka) (Godoy et al., 2018). From all the volcanoes in the volcanic chain, Paniri shows the oldest eruption age ($^{40}Ar/^{39}Ar$ ages) at 1.39±0.29 Ma (Godoy et al., 2017).

Eruptive history and units from Paniri

Phase I

The first evolutionary phase of Paniri volcano is made up of two units, namely Malku and Los Gordos. Though there is no geochronological dating performed at Malku, an $^{40}Ar/^{39}Ar$ age of 1.39 ± 0.29 Ma was obtained for Los Gordos unit, which was erupted after Malku, therefore becoming the minimum suggested age for Malku (Godoy et al., 2017). This phase of eruption in the construction of Paniri is the Plateau shield. It is the most enduring and most voluminous phase of eruption of the volcano with a total volume of ~51 km^3 (Godoy et al., 2018). Malku is mainly composed of eroded lava flows and outcrops in the north-west zone of the volcanic edifice. Outcropping at ~12 km maximum distance from the volcanic vent, this unit is the most radially distributed unit above the ignimbrite basement. The geochemical composition of the Malku unit varies from andesitic to trachy-dacitic (Godoy et al., 2018).

Los Gordos unit flows extend almost radially up to ~9 km and outcrop in the north and north-western zone of the volcanic edifice overlying Malku. This unit consists mainly of pyroclastic deposits and autobrecciated lava flows which are blocky and thicker than those of Malku (Godoy et al., 2018). An age of 1.39 ± 0.29 Ma was assigned to this layer using a $^{40}Ar/^{39}Ar$ dating method on amphibole minerals, and a minimum age of 0.8 Ma from the dating of the third layer to be deposited in this area, the Las Lenguas unit.

Phase II

The second evolutionary phase of Paniri volcano is made up of erupted lavas and thin pyroclastic deposits of Las Lenguas and isolated flows from the Las Negras unit (Godoy et al., 2018). This phase is considered to be the "Main Edifice" stage, with lavas showing flow-banding textures and are highly eroded (Godoy et al., 2018). The Las Lenguas unit covers almost all the flows from the Malku and Los Gordos units, lavas and pyroclastic flows from the Plateau shield phase, out-cropping and reaching distances between 5 and 12 km from the volcanic vent. The

chemical composition of Los Gordos varies between andesitic to dacitic (Godoy et al., 2018), with $^{40}Ar/^{39}Ar$ ages of 640 ± 140 ka and 620 ± 90 ka (Godoy et al., 2017), while K/Ar ages of 400 ± 100 ka and 500 ± 100 ka were obtained by Seelenfreund et al. (2009).

The exposure of the Las Negras unit at Paniri is restricted to the north-western flanks of Crater II. The chemical composition of lava flows from the Las Negras unit varies between basaltic-andesite to andesite (Godoy et al., 2018), with an $^{40}Ar/^{39}Ar$ age of 402 ± 46 ka obtained from one lava flow (Godoy et al., 2017).

Phase III

The third eruption phase at Paniri is known as the Old Cone phase. It corresponds to the southeast cone construction recognized on the volcanic edifice and it is characterised by lavas from the Viscacha unit. The analysed lava flows from the Viscachas unit (Pv) are dacitic to rhyolitic in composition, with flow banding textures and andesitic inclusions (Godoy et al., 2018). Godoy et al. (2017) obtained an $^{40}Ar/^{39}Ar$ age of 325 ± 8 ka, and Seelenfreund et al. (2009) a K/Ar age of 300 ± 100 ka from this unit.

Phase IV

The last two layers at Paniri, Laguna (Pla) and Llareta (Pll), make up the fourth eruption phase. This eruption phase corresponds with the north-westward migration of the eruption vent and was characterised by construction of two different craters, i.e., Crater II and Crater III (Godoy et al., 2018). This gave rise to the Laguna unit. Laguna is mainly made up of lava and pyroclastic deposits which are distributed along the north-western flank of the volcano (Godoy et al., 2018). Godoy et al. (2018) published one new $^{40}Ar/^{39}Ar$ age for this layer at 169 ± 5 ka, and this layer is dacitic in composition.

The Llareta unit is made of lobate lavas erupted from the last volcanic vent and they flowed to the north-eastern and southwestern flanks of the volcano (Godoy et al., 2018). The published $^{40}Ar/^{39}Ar$ ages for Llareta unit are 150 ± 6, 164 ± 3 ka, and 264 ± 99 ka (Godoy et al., 2017). Its chemical composition varies between andesite to dacite.

2.2.3. Toconce Volcano

Toconce volcano (Figure 9) is a composite Late Pleistocene – Holocene age stratovolcano located at 22°11’17’’S, 68°04’43’’W with an approximate height of 5 335 m and is located at the center of the SPLVC (Ramirez and Huete, 1981; Marinovic and Lahsen, 1984; López et al., 2012, Polanco et al., 2012). Toconce has a central crater, and its evolution can be divided into three different stages which are all dacitic-andesitic (varying between 57 and 67% by weight of SiO_2) in composition (López et al., 2012). Toconce is constructed on top of the Toconce ignimbrite (belonging to the Toconce Formation) and Sifon ignimbrite, and these ignimbrites both belong to the dacite-rhyolite ignimbrite sequences related to the APVC. Lavas from Toconce are primarily composed of plagioclase and glass, with amphibole, biotite, pyroxene, and quarts making up the rest (López et al., 2012, Polanco et al., 2012). Very little is known about Toconce, the available ages for Toconce are 1.1 ± 0.1 Ma (Francis and Baker, 1977; Marinovic and Lahsen, 1984) and 0.959 ± 0.005 Ma (Godoy at el., 2017) assigning the volcano to a Pleistocene age.

López et al. (2012) investigated the evolution of the Toconce volcanic system (Antofagasta Region) through the interpretation of aerial photographs, macro and microscopic description of rocks and their geochemical characterisation. They established that the evolution of the Toconce volcano occurred over three different evolutionary stages/phases.

Phase I
The first phase was dominated by the eruption of lava flows deposited on the basement corresponding to the Toconce ignimbrite.

Phase II
The middle/intermediate phase is characterised by great volumes of andesitic lavas that show up on the NNE and SSE flanks.

Phase III
The final stage is when most of the volcanic structure was constructed. This is where deposits of moraines associated with the last glacial events between 15 000 - 1 000 years ago in the altiplanos. The moraines are deposited at elevations above 4 300

m and they developed as a result of glacial erosion (López et al., 2012, Polanco et al., 2012).

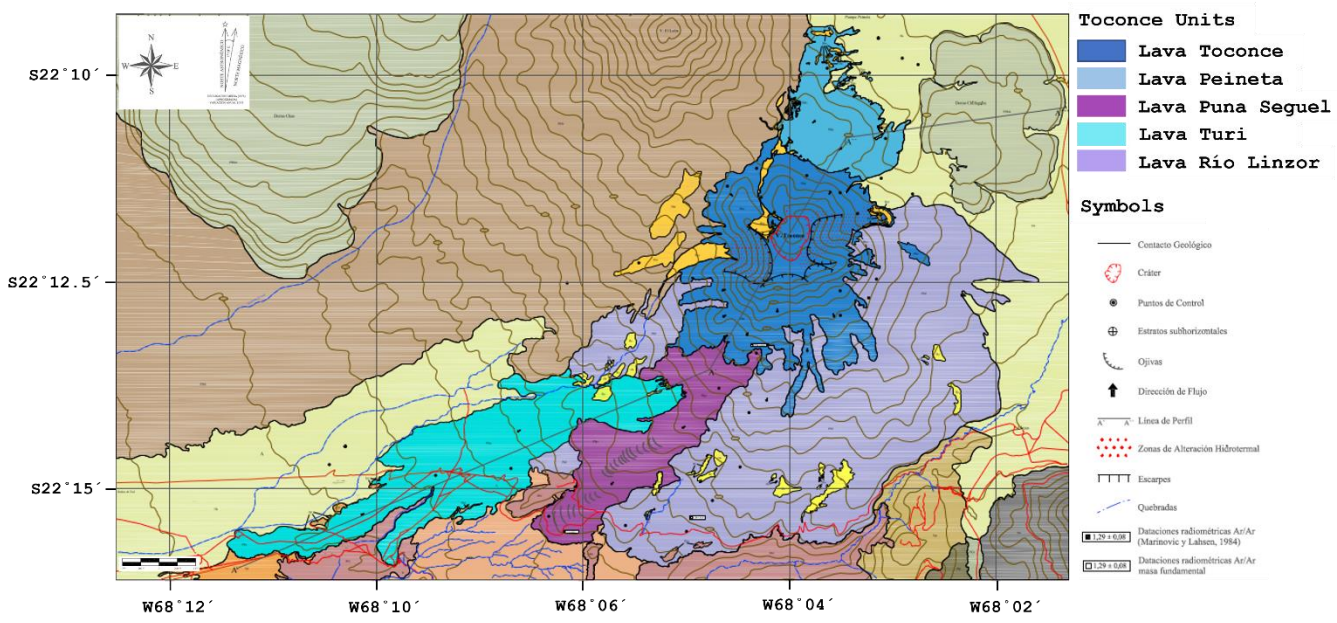

Figure 9. Geological map of Toconce.

3. Methods

3.1. Sample selection and preparation

A total of 12 lava flows/eruptive units from Paniri (7 units) and Toconce (5 units) were sampled for further boron isotope analyses. Due to accessibility to of the units, 7 samples were taken from Paniri, 1 sample from each unit Llareta (Pani-16-02), Laguna (Pani-12-10), Viscacha (Pani-12-08), Las Negras (Pani-05), Las Lenguas (Pani-12-06b), Los Gordos (Pani-14-03), and Malku (Pani-01). 8 samples were taken from Toconce, 2 samples from each Lava Toconce (TOC-15-03 & TOC-15-04), Lava Pieneta (TOC-12-01 & TOC-12-04), Lava Turi (TOC-12-10 & TOC-19-01), And 1 sample from Lava Puna Seguel (TOC-22-03) and Lava Rio Linzor (TOC-22-05). Although there exist contextual geochemical data for Paniri and Toconce (e.g, Godoy et al., 2017 and 2018; González-Maurel et al., 2019a and 2019b), this work aims to provide a comprehensive geochemical characterisation of the sampled lava flows. The goal is thus to allow the boron isotope data to be interpreted in a well-characterised framework and establish a coherent geochemically analysed sample set from each volcano. New and published geochemical and isotope data are presented in Section 4.

Rock samples (7 rock samples from Paniri and 8 rock samples from Toconce) were carefully selected and separated, then crushed using the primary and jaw crusher available at the Department of Geological Sciences, UCT. A fraction of the crushed rock samples was used for mineral separation (e.g., clinopyroxene and olivine), and used for $\delta^{18}O$ analyses. The remaining fraction was sent for milling using an agate mill to obtain powders for bulk rock analyses as described below.

3.2. X-Ray Fluorescence (XRF)

Claisse-Fluxy Fusion Discs

The samples used were prepared into fusion discs and pellets for XRF analyses. The fusion discs used to analyse for major elements were prepared by weighing 2 g of powdered sample and added into a crucible of known mass and dried in an oven, at 110°C, for at least 4 hours. The samples were then cooled, re-weighed, and put in a furnace at a temperature between 850-1000°C overnight. A

final re-weighing of the samples was performed before transferring them from the crucibles into small glass vials that were then sealed with mylar film and a lid.

Lithium tetraborate flux was dried in a furnace overnight at 450°C and was allowed to cool. The 6 g of the cooled flux was used as a releasing agent, and 0.7 g from each sample was measured into labelled vials/glass tubes and sealed with mylar film and lid. The samples and flux were fused together in a Claisse gas burner to form fusion discs.

XRF pellets

XRF pellets used for the analysis for trace elements were prepared by weighing 6 g of powdered sample and mixed with 3 drops of binding agent. The weighed powder samples and the binding agent were mixed thoroughly, and a small test tube of boric acid was added to the mould and a cylinder inserted. A hydraulic press was used to apply pressure of about 10 tons on the palled and the pellet was removed from the mould and labelled accordingly.

XRF Analysis

The XRF analyses for major and trace elements was performed using a Panalytical Axios XRF spectrometer, in the Department of Geological Sciences at the University of Cape Town. The samples were analysed for bulk rock major oxides and trace elements separately but were both calibrated using a series of well characterised standards from the United States Geological Survey, MINTEK, and the Geological Society of Japan. These standards were prepared in a similar way as the samples analysed. Calibrations and corrections were applied on elemental concentrations, enhancement effects, absorption, and spectral line overlap. Typical internal two-sigma analytical errors for individual analyses were < 2 %RSD for XRF.

3.3. MC-ICP-MS

The radiogenic isotope analyses were performed with the Nu Instruments NuPlasma HR in the MC-ICP-MS facility, housed in the Department of Geological Sciences, University of Cape Town. The method of analyses is well described in detail by Harris et al., (2015) and Howarth et al., (2019). Strontium (Sr) was analysed as 200 ppb 0.2% HNO_3 solutions using NIST SRM987 as the reference standard, with a normalising value for $^{87}Sr/^{86}Sr$ of 0.710255.

Strontium data were corrected for Rb interference, using the measured signal for ^{85}Rb and the natural $^{85}Rb/^{87}Rb$ ratio, and instrumental mass fractionation, using the exponential law and an $^{86}Sr/^{88}Sr$ value of 0.1194. Neodymium was analysed as 50 ppb 2% HNO_3 solutions using Nu Instruments DSN-100 desolvating nebuliser with JNdi-1 as reference standard, after Tanaka et al. (2000). The normalising value of JNdi-1, for $^{143}Nd/^{144}Nd$, is 0.512115. Neodymium isotope data were corrected for Sm and Ce interference, using the measured signals for ^{147}Sm and ^{140}Ce and the natural Sm and Ce isotope abundances, and instrumental mass fractionation, using the exponential law and a $^{146}Nd/^{144}Nd$ value of 0.7219. Lead (Pb) isotope analyses used NIST SRM981 as reference standard, with $^{208}Pb/^{204}Pb$, $^{207}Pb/^{204}Pb$, $^{206}Pb/^{204}Pb$ reference values of 36.7219, 15.4963 and 16.9405. Pb isotope data was corrected using the reference $^{205}Tl/^{203}Tl$ and exponential law to correct for instrumental mass fractionation. Typical internal two-sigma analytical errors for individual analyses were < 3 %RSD for ICP-MS.

3.4. Laser fluorination

Laser fluorination (LF) for oxygen isotope analyses was performed on olivine and pyroxene grains following the method fully described by Harris & Vogeli (2011). Grains of olivine and pyroxene that were visibly free of alteration were selected by hand-picking under a binocular microscope. The system uses a 25 W (at full capacity) New Wave CO_2 laser, that is mounted on a movable stage, taking a normal load of 10 samples and 2 standards in a highly polished sample holder of pure Ni.

After loading the samples into the sample holder, they are placed into an oven at 110°C for at least an hour (to remove any absorbed moisture from the sample), then moved into a reaction chamber. Once they are loaded into the chamber, the samples are exposed to 10Kpa of BrF_5 in two stages. In the first stage, the samples were exposed to BrF_5 for 30s then followed by a cryogenic removal of BrF_5 and >30mins of chamber pumping. In the second stage, the BrF_5 is left over night and once the reaction is complete, any excess BrF_5 and free Br are allowed to pass through a KCL filter (at 200°C) that retains F_2 that has been produced. The pure O_2 was collected using glass bottles containing 5Å molecular sieve for storage and frozen into Liquid Nitrogen. The oxygen isotope results are reported in standard δ-notation relative to V-SMOW

(Vienna Standard Mean Ocean Water) where $\delta=[(\delta^{18}O/\delta^{16}O)$ sample/$(\delta^{18}O/\delta^{16}O)$ V-SMOW – 1] *1000.

Measured values of the UCT in-house standard MON GT (Monastery garnet, $\delta^{18}O$ = 5.38‰) were used to normalise the raw data and correct for drift in the reference gas. The $\delta^{18}O$ value of MON GT was established by cross-calibration with the UWG-2 garnet standard of Valley et al. and San Carlos olivine. The long-term average difference in $\delta^{18}O$ values of duplicates of MON GT is 0.15‰, which corresponds to a 2σ S.D. value of 0.15‰. Laser fluorination data are given in Table 1. All analyses gave gas pressures of O_2 that were consistent with ~100% conversion of mineral to O_2.

3.5. LA ICP-MS for trace elements in nano-pellets

Sample powders were shipped to Kiel University, Germany, where further processing was done with a Fritsch Pulverisette 7 PL mill. Following slightly modified protocols of the method established by Garbe-Schönberg and Müller (2014), ±3 g of each of the finer-milled powdered rock samples were made into nano-particulate pressed pellets, commonly called “nano-pellets”.

The multi-trace element abundances of these nano-pellets were analysed at the ICPMS-Lab, Institute of Geosciences, Kiel University, Germany with an Agilent 8900 ICP-MS coupled to a Coherent 193 193 nm GeoLas HD laser ablation system, as described in Garbe-Schönberg and Müller (2014). Five spots were analysed on each nano-pellet to assess homogeneity, and the average analytical precision for all elements analysed was 2.6% RSD (1SD) and 2.8% RSD for boron. Replicate analyses of the samples over the length of each analytical session gave an average measurement uncertainty of the samples of 2.6% RSD for all trace elements but increased to 9.5% RSD for boron. This method was recent used in Godoy et al. (2023).

3.6. LA MC-ICP-MS for B-isotopes in nano-pellets

Following the same approach as in Godoy et al (2023), after the trace element analyses at Kiel University, the nano-pellets were shipped to the Department of Geological Sciences, University of Cape Town, where boron isotope analyses were done using an ASI RESOlution 193 nm laser ablation system coupled to a Nu

Instruments NuPlasma HR MC-ICP-MS operating at 6 kV and fitted with a light-element, high abundance skimmer cone. The laser analysis used a 220 µm spot size ablating along a 450 µm line at 6 $\mu m.sec^{-1}$, after first rapidly sweeping the surface clean with a 240 µm laser spot. The energy of the laser was set to 1.2 kV giving an energy density of ±4.3 $J.cm^{-2}$. The sample cell was flooded with high-purity helium at 400 $ml.min^{-1}$ and high-purity nitrogen at 9 $ml.min^{-1}$ during laser ablation. The gas stream from the sample cell was mixed with high-purity argon before reaching the plasma.

Analyses of JB-2 reference material nano-pellets with a known $\delta^{11}B$ value of +7.12 ± 0.20 per mill was used to bracket each analysis of the unknown samples, and allowed the referencing of the $\delta^{11}B$ data to a value of 4.04362 ± 0.001 for $^{11}B/^{10}B$ for NIST SRM951 (Liu et al, 2018). Each nano-pellet sample was analysed 4 times in succession, and the final $\delta^{11}B$ value is the average of these repeat analysis. The 2σ reproducibility values listed in Table 6 are based on these repeat analyses, and propagating the uncertainty of the JB-2 and NIST SRM951 reference values giving very robust and conservative estimates of precision. This method was recent used in Godoy et al. (2023).

Prior to the analysis of the Toconce and Paniri samples for $\delta^{11}B$ compositions, nano-pellets produced for a number of geological reference materials with boron isotope compositions listed in the GeoReM database were analysed by LA MC-ICP-MS using this method. The resulting agreement between the $\delta^{11}B$ data obtained using this method and the data in the GeoReM database is illustrated in Figure 10. It can be seen that this method gives good results and provide confidence in the $\delta^{11}B$ data for the samples from Toconce and Paniri.

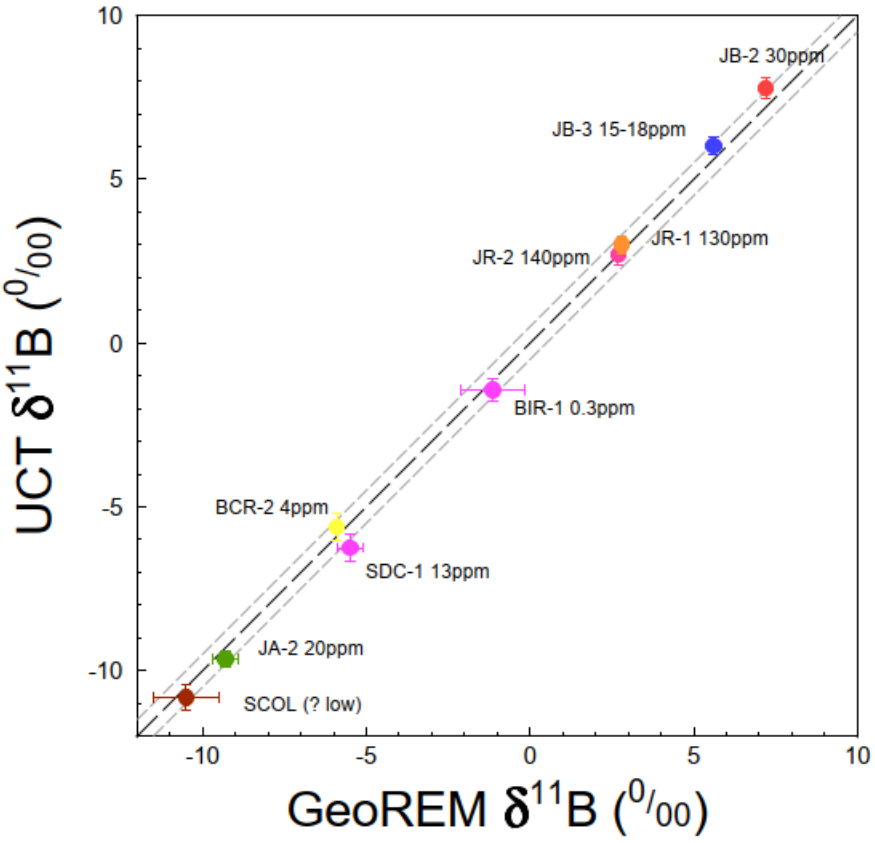

Figure 10. UCT δ11B vs GeoREM δ11B plot of geological reference material with known values from GeoReM database.

4. Results

The comprehensive geochemical dataset generated in this project for samples from each eruptive unit at Paniri and at Toconce will be discussed here within the broader context of the APVC and the SPLVC. The goal is to place these volcanoes in the local geochemical context of published interpretations and models to enable the main focus of the project, boron isotope systematics.

4.1. Major and Trace Element data

The major element data as determined by XRF analyses are presented in Table 1, and are well constrained within the local context (Godoy et al.,2017). Paniri samples have high SiO_2 (56.04 - 66.08 wt.%) with moderate alkali (Na_2O + K_2O: 5.93 - 7.29 wt.%), while Toconce samples have high SiO_2 (56.53 - 66.08 wt.%) with moderate alkali (Na_2O + K_2O: 5.25 - 7.44 wt.%). Na_2O + K_2O shows a positive correlation with SiO_2, with a correlation

coefficient (R^2) = 0.94 (Pani) and 0.95 (Toc). The observed trend is comparable with to that of the volcanoes in the local geological context (see Figure 11).

Table 1(a): New major element XRF data for Toconce obtained from nano-pellet analysis, and existing major element XRF data for Paniri.

wt%	TOC-15-03	TOC-15-04	TOC-12-01	TOC-12-04	TOC-22-03	TOC-12-10	TOC-19-01	TOC-22-05	Pani-01	Pani-14-03	Pani-12-06b	Pani-05	Pani-12-08	Pani-12-10	Pani-16-02
SiO_2	62.85	63.67	65.96	63.84	63.92	56.53	56.53	66.14	57.96	63.2	66.08	56.04	64.66	65.96	63.77
TiO_2	0.53	0.51	0.49	0.63	0.61	0.8	0.8	0.49	0.83	0.6	0.5	0.86	0.67	0.63	0.58
Al_2O_3	17.4	16.64	15.25	16.29	15.77	15.86	15.86	14.45	16.54	16.61	15.53	16.87	15.53	15.28	15.59
Fe_2O_3	3.64	3.78	3.42	4.26	4.14	7.22	7.22	3.34	6.19	4.35	3.13	7.06	4.37	3.93	4.34
MnO	0.08	0.07	0.06	0.07	0.07	0.13	0.13	0.06	0.09	0.07	0.05	0.11	0.07	0.06	0.07
MgO	1.14	1.56	1.44	1.93	1.85	4.88	4.88	1.31	3.01	1.58	1.04	4.09	2	1.25	2.15
CaO	4.31	4.57	3.38	4.2	4.26	6.8	6.8	2.94	5.99	4.23	3.27	7.37	4.49	3.69	4.16
Na_2O	4.02	3.87	3.3	3.9	3.46	3.32	3.32	3.07	3.49	3.89	3.5	3.49	3.75	3.84	3.52
K_2O	2.89	3.12	3.69	2.99	3.33	1.93	1.93	4.36	2.44	3.07	3.75	1.91	2.98	3.45	3.49
P_2O_5	0.15	0.14	0.13	0.17	0.17	0.21	0.21	0.14	0.22	0.16	0.15	0.21	0.16	0.16	0.15
SO_3	0	0	0	0	0	0	0	0	0.02	-	-	0.22	-	-	-
Cr_2O_3	0.01	0	0.01	0.01	0.01	0.02	0.02	0	0.01	-	-	0.01	-	-	-
NiO	0.01	0.01	0.01	0.01	0.01	0.02	0.02	0.01	0.01	-	-	0.01	-	-	-
H_2O-	0.08	0.03	0.13	0.02	0.08	0.09	0.09	0.03	0.23	-	-	0.23	-	-	-
LOI	1.63	0.22	1.22	0.41	1.06	0.87	0.87	1.72	1.95	-	-	1.02	-	-	-
Total	**98.74**	**98.18**	**98.48**	**98.7**	**98.73**	**98.71**	**98.71**	**98.06**	**98.96**	**97.33**	**96.7**	**99.51**	**98.24**	**97.86**	**97.37**
References									González-Maurel et al., 2019	Godoy et al., 2018	Godoy et al., 2018	González-Maurel et al., 2019	Godoy et al., 2018	Godoy et al., 2018	Godoy et al., 2018

The samples from Paniri and Toconce show a compositional variation along the TAS diagram, with Paniri varying from andesitic-to-dacitic and basaltic-andesite to andesite at Toconce, and lavas from the SPLVC display a calc-alkaline trend that varies from basaltic-andesite to dacite in composition (Figure 11) (Godoy et al., 2014). The samples presented in this work are plotted in context of volcanoes from the SPLVC (after Godoy et.al., 2014 and 2017), and they fit-in well within the context of the already published studies of SLPVC volcanoes.

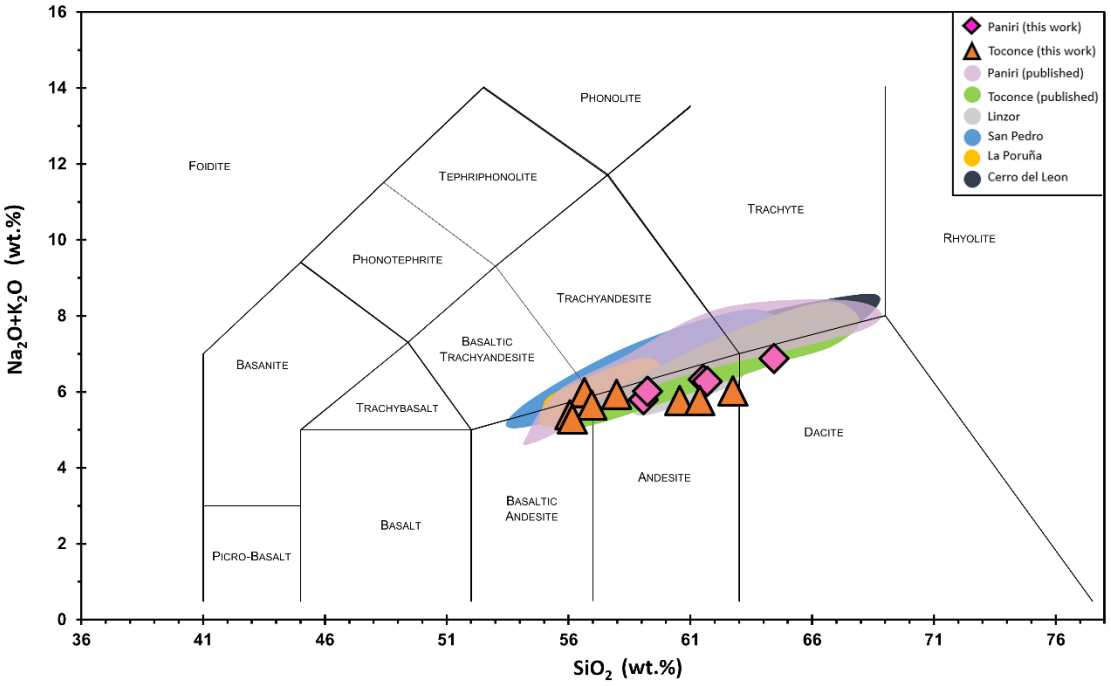

Figure 11. Total-Alkali vs. Silica (TAS) diagram for sampled lavas from Paniri and Toconce plotted with volcanoes from the San Pedro-Linzor Chain (after Godoy et al. (2014), coloured fields). The samples show well-defined sub-alkaline trends, varying from andesitic to dacitic at Paniri, and basaltic-andesite to andesite at Toconce, in composition.

Table 2: New LA-ICP-MS trace element data (ppm) for Toconce samples obtained from nano-pellet analysis.

	TOC-15-03	TOC-15-04	TOC-12-01	TOC-12-04	TOC-22-03	TOC-12-10	TOC-19-01	TOC-22-05
Li	32.8	39.5	50.4	21.7	40.8	58.3	19.4	54.9
Be	3.06	3.66	3.00	2.32	3.00	3.50	1.71	3.71
B	33.5	36.3	83.5	19.7	52.2	69.4	29.2	79.1
Sc	11.57	13.08	8.66	11.17	11.04	9.92	18.92	9.68
V	83.5	112	59.2	64.5	106	66.5	168	77.4
Cr	34.6	40.5	54.3	58.2	54.9	48.1	126	42.5
Mn	659	544	458	551	525	452	856	444
Co	9.82	9.80	6.20	9.48	9.59	6.59	22.8	6.23
Ni	18.23	11.23	5.87	11.66	13.96	7.48	52.8	7.63
Cu	20.4	46.8	8.67	19.82	19.30	23.1	34.1	27.3
Zn	87.0	92.3	63.1	80. 9	82.9	63.3	86.5	64.4
Ga	23.6	25.5	18.3	21.3	21.8	20.7	20.1	17.6
Rb	179	245	180	131	195	218	70.0	250
Sr	475	432	291	417	384	279	472	228
Y	19.98	22.6	14.71	14.80	19.04	17.54	17.06	21.0
Zr	216	276	151	167	254	197	140	256
Nb	14.10	16.48	13.10	11.42	15.20	15.06	8.58	15.89
Mo	2.21	4.00	6.47	0.84	5.04	4.90	2.62	6.12
Cs	8.15	13.48	18.48	3.79	16.00	20.1	3.78	23.2
Ba	923	864	611	732	760	745	592	646
La	38.7	43.8	34.2	30.3	38.5	34.6	22.3	37.9
Ce	76.8	90.8	67.5	62.6	76.4	76.0	44.2	73.7
Pr	8.72	10.11	7.18	7.12	8.91	7.86	5.51	8.50
Nd	32.1	36.5	24.7	25.9	32.4	27.3	21.6	30.6
Sm	5.58	6.67	4.38	4.77	5.98	4.86	4.38	5.57
Eu	1.18	1.20	0.85	1.05	1.10	0.94	1.10	0.91
Gd	4.56	5.26	3.41	3.73	4.71	3.83	3.81	4.46
Tb	0.63	0.75	0.47	0.52	0.65	0.56	0.56	0.65
Dy	3.48	4.11	2.68	2.86	3.57	3.18	3.23	3.74
Ho	0.68	0.79	0.51	0.53	0.67	0.62	0.63	0.73
Er	1.85	2.14	1.41	1.42	1.80	1.73	1.72	2.04
Tm	0.27	0.31	0.22	0.21	0.26	0.26	0.25	0.31
Yb	1.69	1.98	1.47	1.30	1.66	1.76	1.56	2.00
Lu	0.26	0.29	0.23	0.19	0.24	0.26	0.23	0.30
Hf	5.74	7.56	4.45	4.45	6.69	5.27	3.59	6.83
Ta	1.17	1.51	1.61	0.89	1.31	1.44	0.58	1.60
W	5.34	6.16	5.06	1.28	5.96	3.59	3.77	7.23
Bi	0.03	0.04	0.22	0.07	0.09	0.46	0.05	0.45
Th	18.73	27.6	28.7	14.32	23.0	24.5	7.27	26.5
U	5.82	9.42	12.42	3.61	7.27	8.34	1.98	8.81

Table 3: New LA-ICP-MS trace element data (ppm) for Paniri samples obtained from nano-pellet analysis.

	Pani-01	Pani-14-03	Pani-12-06b	Pani-05	Pani-12-08	Pani-12-10	Pani-16-02
Li	24.9	29.0	31.6	15.9	25.4	33.5	32.4
Be	1.89	2.26	2.68	1.58	2.30	2.81	2.76
B	34.8	29.4	35.0	20.0	32.6	33.1	50.5
Sc	15.96	12.31	9.53	20.3	12.58	10.69	13.44
V	140	103	64.8	172	110	90.8	115
Cr	60.0	5.81	9.23	63.0	54.4	37.6	59.5
Mn	675	584	404	829	577	525	575
Co	20.0	14.80	11.81	24.9	12.76	9.05	26.0
Ni	22.0	5.16	4.92	30.0	11.68	2.43	19.62
Cu	26.9	16.39	35.2	37.1	15.59	9.81	19.61
Zn	79.2	70.5	74.8	78.4	77.1	78.8	75.9
Ga	20.1	20.9	19.51	19.61	21.8	21.6	22.2
Rb	87.9	131	159	50.7	124	162	184
Sr	481	469	414	547	504	490	458
Y	19.78	18.20	17.00	16.96	17.30	17.40	18.07
Zr	191	185	235	137	204	223	207
Nb	11.15	11.64	12.89	8.28	11.28	13.46	12.91
Mo	2.14	2.62	3.58	1.57	3.18	3.54	4.76
Cs	5.94	5.91	7.09	2.26	4.42	7.18	10.49
Ba	661	796	849	570	826	889	782
La	28.4	29.2	36.9	19.81	30.5	36.3	36.3
Ce	59.4	65.0	74.5	41.3	66.1	75.4	75.4
Pr	27.1	25.8	29.0	20.8	27.2	29.6	29.7
Nd	6.99	7.09	8.12	5.22	7.33	8.24	8.27
Sm	5.27	4.76	5.07	4.20	5.04	5.28	5.20
Eu	1.22	1.04	1.04	1.11	1.12	1.11	1.06
Gd	4.72	3.95	4.12	3.85	4.10	4.27	4.25
Tb	0.69	0.59	0.57	0.57	0.58	0.60	0.62
Dy	3.78	3.23	3.06	3.16	3.14	3.13	3.33
Ho	0.74	0.65	0.60	0.63	0.62	0.61	0.67
Er	1.99	1.80	1.67	1.69	1.66	1.63	1.85
Tm	0.29	0.28	0.25	0.24	0.25	0.24	0.28
Yb	1.84	1.81	1.66	1.54	1.60	1.52	1.79
Lu	0.27	0.28	0.26	0.23	0.25	0.24	0.28
Hf	5.12	4.98	6.37	3.61	5.47	6.10	5.79
Ta	0.76	0.94	1.10	0.53	0.80	1.15	1.17
W	9.05	9.40	8.62	8.66	1.95	1.93	26.4
Bi	0.06	0.08	0.09	0.04	0.08	0.09	0.09
Th	10.25	13.97	20.0	5.28	12.60	17.70	24.3
U	2.39	4.23	4.90	1.25	3.35	4.70	7.34

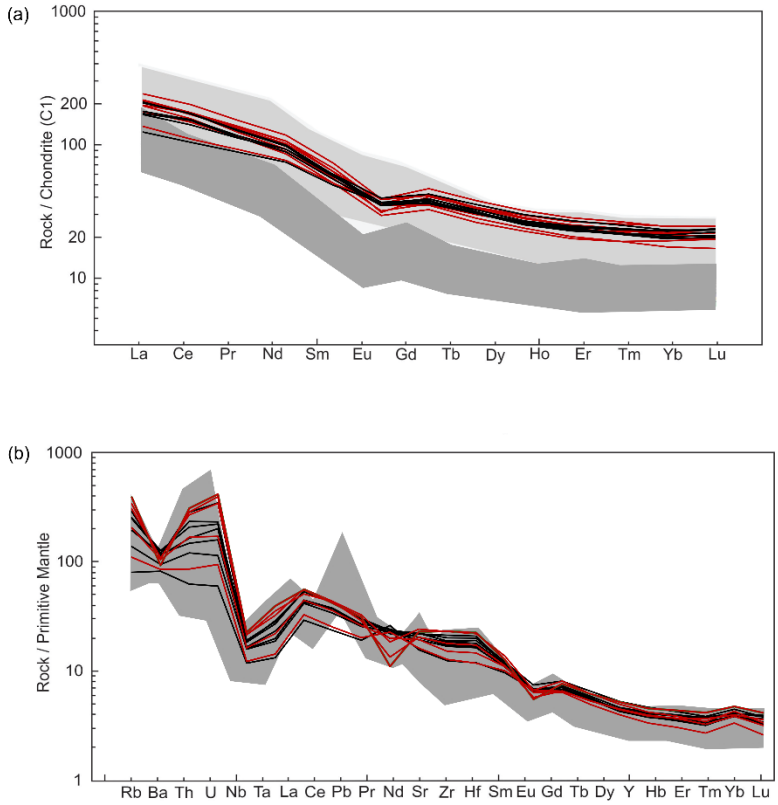

Figure 12. a) REE normalized to chondritic values (after Sun and McDonough, 1989) for representative lava samples at Paniri(black) and Toconce (red). The dark and light grey areas represent normalized composition of lavas erupted in the Central Andes (after (Mamani et al., 2010 and Godoy et al., 2019)). b) Trace elements normalized to primitive mantle diagrams (after Sun & McDonough, 1989) for Paniri(black) and Toconce (red), Gray area represents normalized composition of lavas erupted in the Central Andes (after (Mamani et al., 2010).

For both Paniri and Toconce in general, the chondrite normalized Rare Earth Element (REE) patterns display a moderate enrichment of light-REE (LREE) with small Eu anomalies and fluid-mobile large ion lithophile elements (LILE) (toward the left-end of Figure 12), when compared to the high-REE (HREE) and high-field strength elements (HFSE) (toward the right-end of Figure 12). These are similar to regional magmas, marked grey on the background, from the Central Andes (Mamani et al., 2010).

4.2. Isotope Analyses

4.2.1. Radiogenic Isotopes

A synthesis of new and published (Godoy et al., 2017) $^{87}Sr/^{86}Sr$ and $^{143}Nd/^{144}Nd$ data for samples from Toconce are presented in Table 4, while the published radiogenic isotopes for the selected Paniri samples are also reproduced in Table 4 (Godoy et al., 2018; González-Maurel et al., 2019). $^{87}Sr/^{86}Sr$ ratios for Toconce are the highest in the volcanic chain ranging from 0.7073 to 0.7089. Higher than those of Cerro del Leon, La Poruña, San Pedro and Paniri, presented by Godoy et al. (2014, 2017). Toconce has $^{143}Nd/^{144}Nd$ ratios that are relatively low compared to other volcanoes in the volcanic chain ranging from 0.512275 to 0.512344, more in the range of Cerro del Leon (Godoy et al., 2017).

Table 4: New and published MC-ICP-MS whole-rock radiogenic isotopes data of selected samples from Toconce, as well as published radiogenic isotopes data of selected samples from Paniri.

Volcano	sample name	Reference	$^{87}Sr/^{86}Sr$	±2s	$^{143}Nd/^{144}Nd$	±2s
Paniri	Pani-16-02	Godoy et al., 2018	0.707246	0.000013	0.512340	0.000009
	Pani-12-10	Godoy et al., 2018	0.706909	0.000013	0.512351	0.000010
	Pani-12-08	Godoy et al., 2018	0.707577	0.000012	0.512326	0.000007
	Pani-05	González-Maurel et al., 2019	0.706690	0.000011	0.512374	0.000014
	Pani-12-06b	Godoy et al., 2018	0.707970	0.000014	0.512300	0.000012
	Pani-14-03	Godoy et al., 2018	0.707539	0.000012	0.512344	0.000015
	Pani-01	González-Maurel et al., 2019	0.707539	0.000013	0.512337	0.000012
Toconce	TOC-15-03	this study	0.707666	0.000009	0.512272	0.000010
	TOC-15-04	this study	0.707896	0.000014	0.512275	0.000008
	TOC-12-01	Godoy et al., 2017	0.708836	0.000012	0.512296	0.000011
	TOC-12-04	Godoy et al., 2017	0.707848	0.000001	0.512244	0.000009
	TOC-22-03	this study	0.708165	0.000010	0.512279	0.000012
	TOC-12-10	Godoy et al., 2017	0.708786	0.000012	0.512286	0.000012
	TOC-19-01	this study	0.707351	0.000013	0.512344	0.000010
	TOC-22-05	this study	0.708920	0.000010	0.512278	0.000012

4.2.2. Stable Isotopes

At Paniri $\delta^{18}O$ values were obtained for minerals from three lava flows namely, (i) Malku from olivine (ol) (Pani-01/OGM-23) and clinopyroxene (cpx) (Pani-01), (ii) Los Gordos from cpx (Pani-14-03) and (iii) Llareta from cpx (Pani-16-02). $\delta^{18}O$ values from the analysis of cpx and ol crystals at Paniri ($n_{mineral\text{-}samples} = 4$) ranges from 6.3 to 8.82‰ as presented in Table 5. At Toconce $\delta^{18}O$ values were obtained also for three layers namely, (i) Lava Toconce from plagioclase (plag) (TOC-15-O3 and TOC-15-04), (ii) Lava Puna Seguel from plag and cpx (TOC-22-03), and (iii) Lava Rio Linzor (TOC-22-05). The $\delta^{18}O$ values from the analysis of plag, cpx and bi ($n_{mineral\text{-}samples} = 7$) ranges from 9.12 to 10.91‰ as presented in Table 5. These values fall within the expected range in the context of the CVZ (Michelfielder et al., 2013; Lister, 2019; González-Maurel et al., 2020) magmas and they have values that fall outside of the average mantle values of 5.5 to 5.9‰ (Deegan et al., 2021).

Table 5: New and published laser fluorination O-isotope data for olivine, clinopyroxene and plagioclase crystals from selected eruptive units at Paniri and Toconce. $\delta^{18}O$ data reported in ‰ relative to the V-SMOW scale. Estimations of melt $\delta^{18}O$ values (i.e., $\delta^{18}O_{melt-ol}$, $\delta^{18}O_{melt-cpx}$, and $\delta^{18}O_{melt-plag}$) and calculated using an equilibrium mineral-melt fractionation factor of 1.3‰ for olivine and 0.7‰ for pyroxene (Bindeman et al., 2004) and 0.3‰ for plagioclase (Feeley and Sharp, 1995)

Volcano	Unit	sample name	Reference	$\delta^{18}O_{ol}$	$\delta^{18}O_{ol-melt}$	$\delta^{18}O_{cpx}$	$\delta^{18}O_{cpx-melt}$	$\delta^{18}O_{plag}$	$\delta^{18}O_{plag-melt}$
Paniri	**Llareta**	Pani-16-02	this study	-	-	6.99	7.69	-	-
	Laguna	Pani-12-10	this study	-	-	-	-	-	-
	Viscacha	Pani-12-08	this study	-	-	-	-	-	-
	Las Negras	Pani-05	González-Maurel et al., 2019	-	-	6.3 & 7.0	7.0 & 7.7	-	-
	Las Lenguas	Pani-12-06b	this study	-	-	-	-	-	-
	Los Gordos	Pani-14-03	this study	-	-	7.79	8.49	-	-
	Malku	Pani-01	this study	7.52	8.82	7.94	8.64	-	-
Toconce	**Lava Toconce**	TOC-15-03	this study	-	-	-	-	-	9.63
		TOC-15-04	this study	-	-	-	-	-	9.25
	Lava Pieneta	TOC-12-01	this study	-	-	-	-	-	-
		TOC-12-04	this study	-	-	-	-	-	-
	Lava Puna Seguel	TOC-22-03	this study	-	-	8.42	9.12	9.26	9.56
	Lava Turi	TOC-12-10	this study	-	-	-	-	-	-
		TOC-19-01	this study	-	-	-	-	-	-
	Lava Rio Linzor	TOC-22-05	this study	-	-	10.21	10.91	10.54	10.84

The new B (Table 2 and Table 3) and $\delta^{11}B$ (Table 6) values for the analysed samples vary from 20.0 to 50.5 (ppm) and -6.11‰ (±0.35‰) to +0.23‰ (±0.33‰) for Paniri, and from 19.71 to 83.5(ppm) and -11.16‰ (±0.36‰) to -5.06‰ (±0.49‰) for Toconce. Due to the LA-MC-ICP-MS boron isotope analysis of nanopellet whole rock samples being a new method, the Paniri samples were analysed in duplicate with good agreement between the two sets of data in Table 6. At Toconce, it was possible for some individual (Lava Toconce; and Lava Turi) units to analyse a sample collected close to the flow front and another sample proximal to the vent. As can be seen in Table 6, there is significant and consistent differences in $\delta^{11}B$ values between these vent proximal and distal samples within individual flow units (e.g., Lava Turi: vent-distal sample TOC-12-10 with $\delta^{11}B$ of -11.16 ±0.36‰ versus vent-proximal sample TOC-19-01 with $\delta^{11}B$ -5.06 ±0.49‰).

Table 6: New $\delta^{11}B$ (‰) data for Paniri and Toconce

Volcano	Units	sample name	$\delta^{11}B$	±2s	repeats	$\delta^{11}B$	±2s
Paniri	**Llareta**	Pani-16-02	-0.76	0.32		-0.35	0.25
	Laguna	Pani-12-10	-0.78	0.32		-0.42	0.58
	Viscacha	Pani-12-08	-1.78	0.27		-1.84	0.25
	Las Negras	Pani-05	0.23	0.33		0.39	0.38
	Las Lenguas	Pani-12-06b	-1.29	0.4		-1.35	0.34
	Los Gordos	Pani-14-03	-2.95	0.25		-2.56	0.49
	Malku	Pani-01	-6.11	0.35		-6.68	0.62
Toconce	**Lava Toconce**	TOC-15-03	-7.53	0.32			
		TOC-15-04	-9.33	0.56			
	Lava Pieneta	TOC-12-01	-6.04	0.38			
		TOC-12-04	-6.72	0.66			
	Lava Puna Seguel	TOC-22-03	-6.93	0.41			
	Lava Turi	TOC-12-10	-11.16	0.36			
		TOC-19-01	-5.06	0.49			
	Lava Rio Linzor	TOC-22-05	-10.19	0.32			

5. Discussion

To interpret the new boron isotope data for Paniri and Toconce in this study, it is necessary to present the basic geochemistry of these volcanic centres in the context of petrogenetic models proposed in previous work on the SPLVC including previous B isotope studies in the Andes. The purpose is to present the context for the new boron isotope results which is the main aim of this project and will not reinterpret previous studies.

5.1. Contamination processes

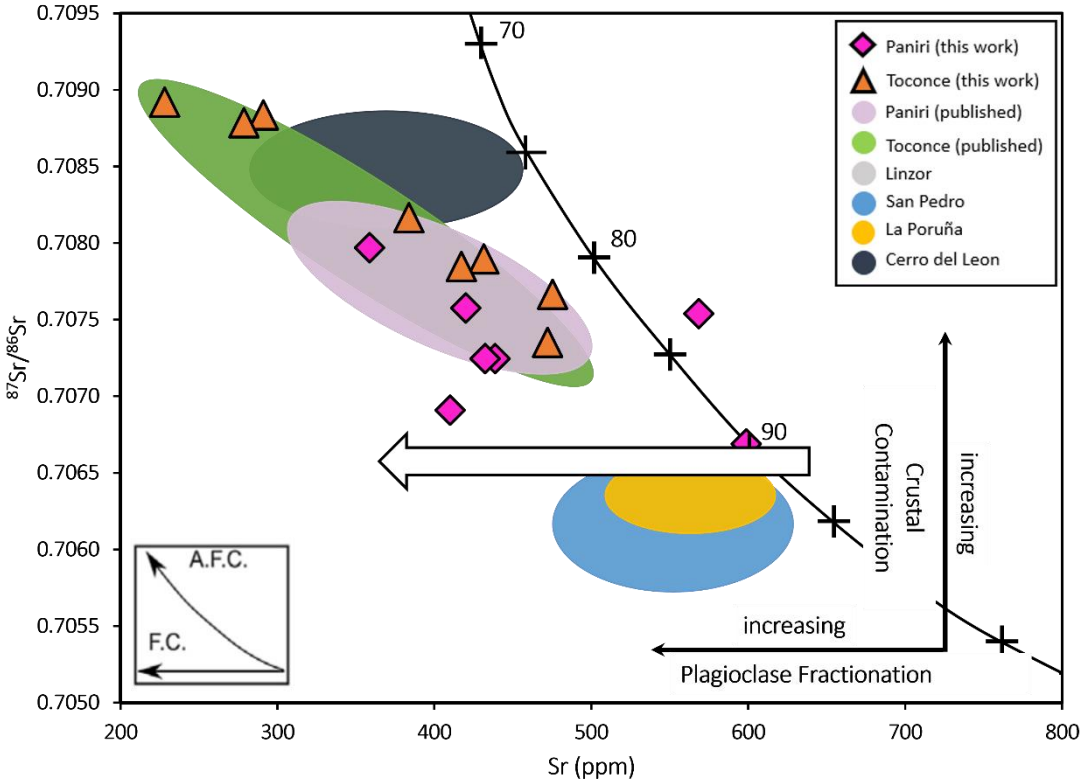

Figure 13. $^{87}Sr/^{86}Sr$ vs Sr (ppm) plot for analysed samples from Paniri, Toconce and the SPLVC (after Godoy et al., 2018). The curve represents the AFC model produced by Godoy et al. (2017). The white arrow represents a proposed trend for closed system fractional crystallization starting from a magma that was initially formed by an AFC process. Values along curve indicate the estimated melt fraction remaining from parent magma.

According to Godoy et al. (2017) Sr characteristics, along the SPLVC, are related to degrees of crustal contamination. The increasing $^{87}Sr/^{86}Sr$ ratios with decreasing Sr are common in the

Andean CVZ (though not characteristic of all composite cones), and as suggested by Godoy et al. (2017) can be interpreted to reflect assimilated proportions of crustal rocks in magmas paired with higher degrees of low-pressure differentiation. The resulting Sr plots (Figure 13 and Figure 14) for Paniri and Toconce agree with the suggestion by Godoy et al. (2017) and González-Maurel et al. (2019b) that along the CVZ (SPLVC specifically) there is more crustal contamination toward the centre of the APMB.

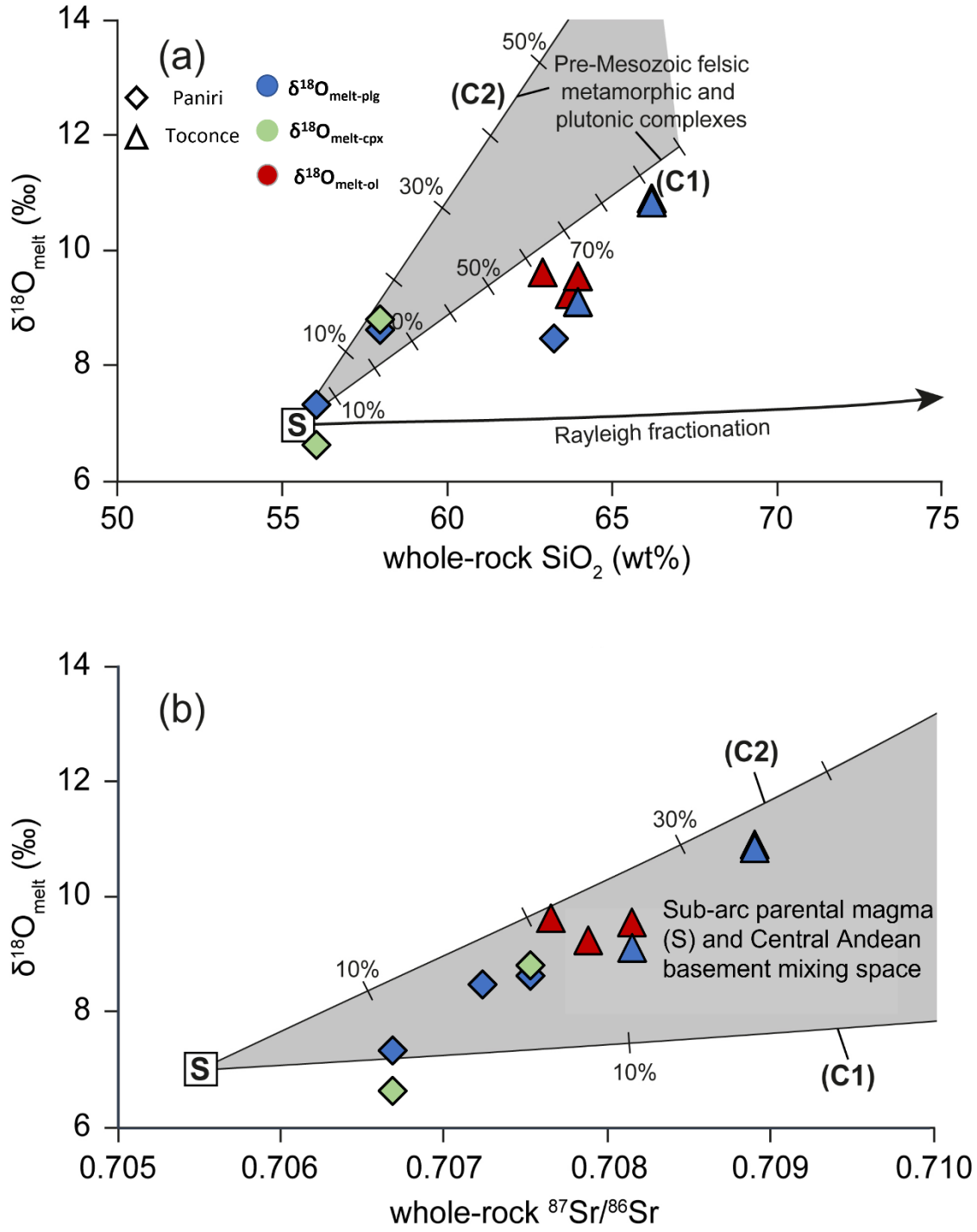

Figure 14. Binary mixing models of $\delta^{18}O$ estimated melt values from plagioclase, clinopyroxene, and olivine (in this work) versus (a) whole-rock SiO_2 and (b) $^{87}Sr/^{86}Sr$ ratios (from this work, Godoy et al., 2018, and González-Maurel et al., 2019). The Rayleigh fractionation trend illustrates the variation in $\delta^{18}O$ values expected from closed-system fractional crystallisation. The model indicates contamination of a starting sub-arc Andean parental magmas (S) by upper Central Andean continental crust considering two crustal compositions: C1 (after Damm et al., 1990) and C2 (after Davidson et al., 1990) (Table 2; after González-Maurel et al., 2020).

$\delta^{18}O$ data for magmas from Paniri range between 6.3 and 8.82‰ and those from Toconce range between 9.12 to 10.91‰ (Table 5), the values overlap and agree with $\delta^{18}O$ values from previously published $\delta^{18}O$ data in the CVZ; e.g., $\delta^{18}O$ values published by (Michelfelder et al., 2013 (7‰ to 9.6‰); Lister, 2018 (7.89‰ to 11.95‰); González-Maurel et al., 2020 (6‰ to 7.9‰); and Sigauke, 2021 (8.6‰ to 10.5‰)). These values all fall outside of the average mantle values of 5.5 to 5.9‰ (Mattey et al., 1994; Iovine et al., 2017) indicating that there has to have been an external source with significantly higher $\delta^{18}O$ values to account for the elevated $\delta^{18}O$ values observed in the CVZ.

It is possible to estimate the $\delta^{18}O$ values of the equilibrium melt by using mineral-melt fractionation factors appropriate for basaltic-andesite (SiO_2 average 55.8 wt% among our samples; Table 1). These are calculated to be $\Delta_{olivine\text{-}melt} = -1.3$, $\Delta_{pyroxene\text{-}melt} = -0.7$ and $\Delta_{plagioclase\text{-}melt} = -0.3$, using the silica-based equations in Bindeman et al. (2004) as applied in González-Maurel et al. (2020). The $\delta^{18}O$ values for both Paniri and Toconce show an increase in $\delta^{18}O$ with an increase in SiO_2 and $^{87}Sr/^{86}Sr$ (Figure 14a and Figure 14b), which is the expected correlation for magmas that have an increase in contamination of the parental magmas progressively towards the centre of the APMB (Godoy et al., 2017; González-Maurel et al., 2020). The data from Paniri and Toconce fits well within the already established measures of crustal assimilation within the CVZ with $^{87}Sr/^{86}Sr$ ratios ranging between 0.7065-0.7080, and $\delta^{18}O$ values ranging from 6‰-11.95‰.

5.2. B contents and $\delta^{11}B$ values in the Central Andes

Previous studies on Central Andean whole-rock samples by Schmitt et al. (2002) obtained an overall $\delta^{11}B$ average of $\delta^{11}B = -3.8\pm2.8$‰ (1 SD) from melt inclusions and matrix glasses of calk-alkaline pumices and lavas from the Neogene-Pleistocene APVC (see Figure 15). Their $\delta^{11}B$ values overlap with the $\delta^{11}B$ range of the local basement rock, $\delta^{11}B = -11$‰ to -5‰ (Kasemann et al., 2000) and are suggested to be indicative of a similar source for B in the APVC ignimbrite magmas, which is dominantly a crustal source (Schmitt et al., 2002). The samples analysed by Schmitt et al. (2002) covered the entire age range from ~10 Ma to 1.3 Ma i.e., Neogene to Pleistocene. Rosner et al. (2003) obtained a wide range of $\delta^{11}B$ values (-7 to +4‰), and B concentrations (6-60 ppm) from late Miocene to Quaternary andesites and dacites from the CVZ (see Figure 15). The positive $\delta^{11}B$ values obtained would need

a source that is more enriched in ^{11}B relative to the mantle and continental crust at $\delta^{11}B$ = -7.1‰ (see Figure 1) and $\delta^{11}B$ = -11‰ to -5‰ (Kasemann et al., 2000) respectively (Rosner et al, 2003). The values obtained by Rosner et al. (2003) progressively decreased as one moves from the front to back-arc with values reaching a low of -7‰. They explained the high $\delta^{11}B$ values observed as seawater-alteration of the upper oceanic crust from the subducted slab. The altered oceanic crust $\delta^{11}B$ values are reflected in the volcanic products (Rosner et al. 2003) and are consistent with Bebout et al. (1999) in that in warm subduction zones (like the Andes) forearc devolatilization is more pronounced and supported by the highly enriched presence of fluid mobile elements, such as B.

Jones et al. (2014) observed a significant variation in $\delta^{11}B$ values from analysed melt inclusions from different time periods, with the Paleocene (~61 Ma) $\delta^{11}B$ values ranging from +0.7±0.9‰ to +3.7±1.2‰, Late Oligocene (~25-23 Ma) $\delta^{11}B$ values ranging from -5.4±1.6‰ to +0.9±1.7‰, and Miocene (~19-17 Ma) $\delta^{11}B$ values ranging from +0.6±1.0‰ to +8.6±1.2‰ (Jones et al., 2009) (Figure 15). They suggested that the range in the $\delta^{11}B$ values from the southern Central Andes reflect a clear time dependence and suggest temporal changes in the sources of boron. Most recently, Godoy et al. (2023) presented whole rock B-concentrations and $\delta^{11}B$ values for La Poruña, ranging from B = 14 to 20 ppm and $\delta^{11}B$ = -1.39±0.54‰(2σ) to +0.94±0.30‰(2σ) (Figure 15). These values overlap with the available boron values within the Central Andes. Using mixing models, that are also used in this thesis, that are based on B and Sr they suggest a two-step magma evolution for La Poruña (Godoy et al., 2023), where the first step supports an interaction of the boron-rich slab derived fluids with mantle-derived primary melts. The second step involves the interaction of ^{11}B-enriched parental magmas with the ^{11}B-depleted continental crust, further modifying the $\delta^{11}B$ values of the parental melts.

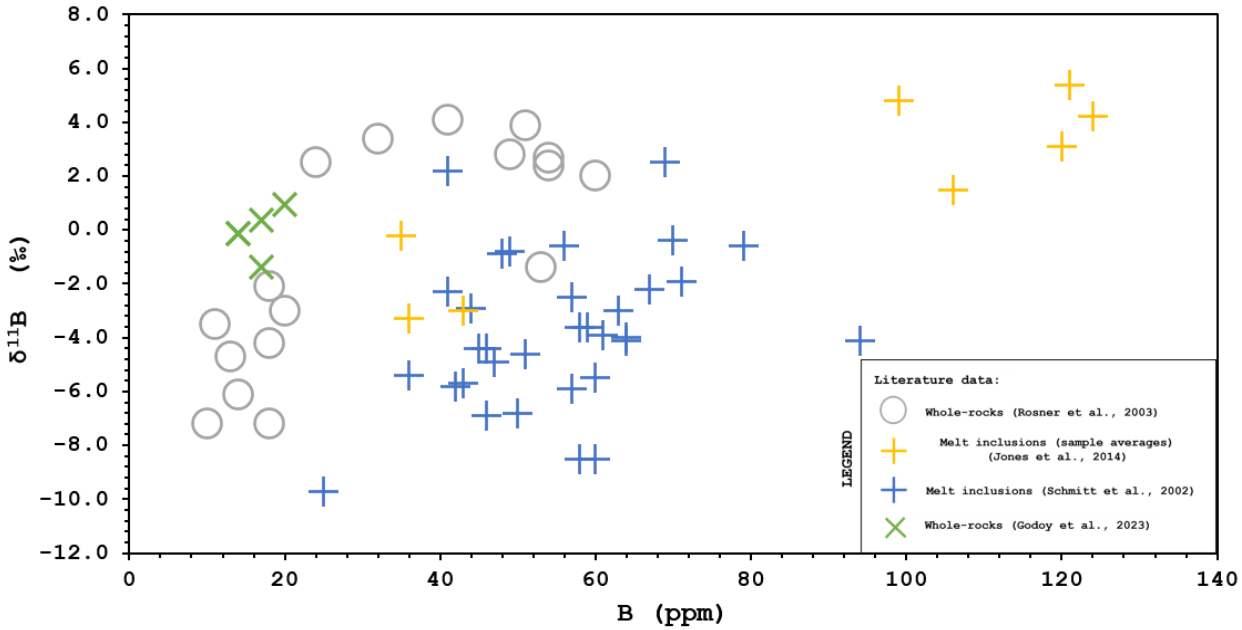

Figure 15. $\delta^{11}B$ values vs B-concentrations of investigated volcanic centres in the Central Andes from Schmitt et al., (2002), Rosner et al., (2003 Jones et al. (2014) and Godoy et al., (2023), uncertainty within symbol size.

5.3. New B contents and $\delta^{11}B$ values overview at Paniri and Toconce

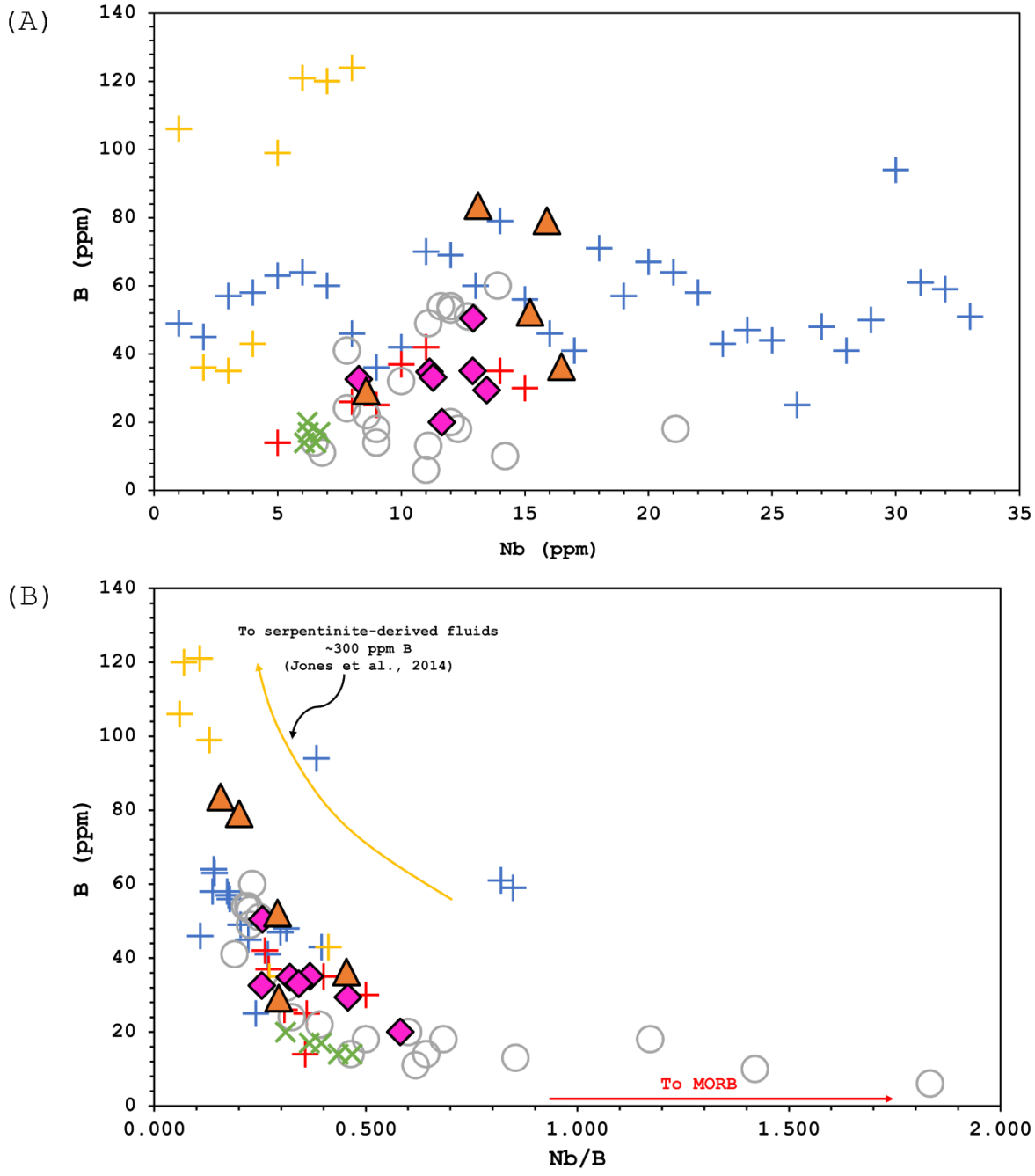

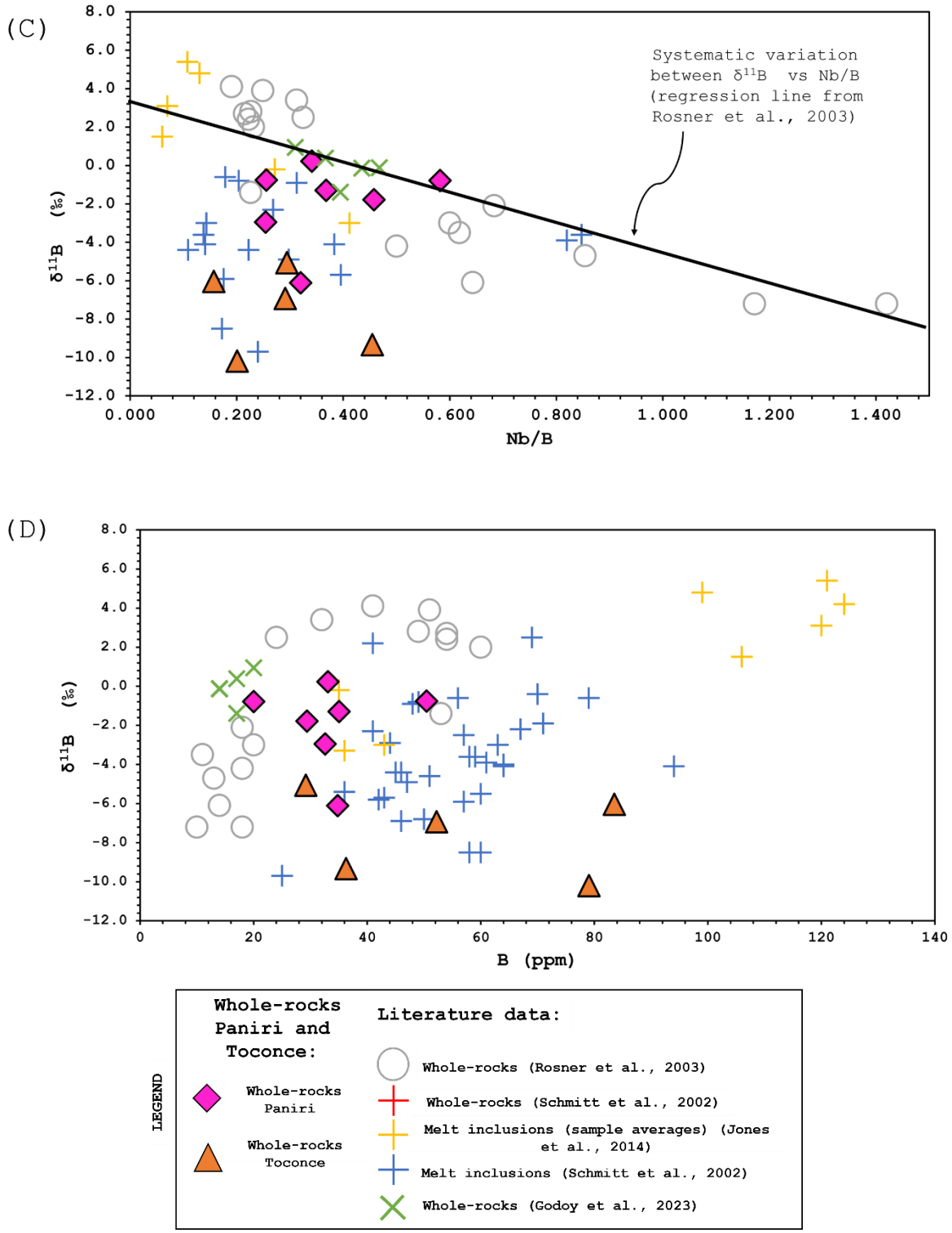

Figure 16. (A) B vs Nb (ppm), (B) B vs Nb/B, (C) δ11B vs Nb/B, and (D) δ11B vs B of Paniri and Toconce plotted in context of investigated volcanic centres in the Central Andes from Schmitt et al., (2002), Rosner et al., (2003), Jones et al. (2014) and Godoy et al., (2023).

In the context of the Central Andes, the B contents and $\delta^{11}B$ values from both Paniri and Toconce overlap with the already existing and published data (Figure 16A, B, C, and D). The B contents at Paniri average at about 33 ppm, with $\delta^{11}B$ values averaging at -1.92‰ and there is no apparent correlation/relationship between the plotted B contents and $\delta^{11}B$ values (Figure 16D). B contents at Toconce average at 50 ppm, with $\delta^{11}B$ values averaging at -7.8‰ and there is a strong negative correlation between B contents and $\delta^{11}B$ values (Figure 16D).

Nb/B ratio is a good proxy for fluid transfers at subduction zones (de Hoog and Savov, 2018; Ishikawa and Tera, 1997), the strong negative correlation between B vs Nb/B (Figure 16B) shows the contribution of a slab derived fluid at Paniri and Toconce (e.g., de Hoog and Savov, 2018; Ishikawa and Tera, 1997). The $\delta^{11}B$ data at Paniri and Toconce agree and overlap with the limited $\delta^{11}B$ data from other volcanoes in the CVZ region (Figure 16C, D).

5.3.1. Paniri B contents and $\delta^{11}B$ values

Boron concentrations at Paniri are heterogeneous, ranging between 20 to 50 ppm and the $\delta^{11}B$ values between -6.11‰ and +0.23‰. When looking at the various reservoirs of B isotopes and elemental concentrations (Figure 1) it is observed that most of these $\delta^{11}B$ values fall outside of the expected volcanic arc $\delta^{11}B$ values ($\delta^{11}B$ -11 ‰ to -5 ‰), with only one unit at Paniri with a $\delta^{11}B$ value of -6.11‰ falling within this range. All the $\delta^{11}B$ values are higher than those of depleted mantle at $\delta^{11}B$ = -7.1‰ (de Hoog and Savov, 2018). For such high $\delta^{11}B$ values reflected in arc settings, it is generally understood that there should be an external source with high $\delta^{11}B$ values, e.g., the AOC which has a wide B concentration and $\delta^{11}B$ compositional range from 0 to +18‰ (de Hoog and Savov, 2018; Fig 9) or -4 to +25‰ (Smith et al., 1995).

A striking feature at Paniri is the two layers, Malku (oldest unit in the SPLVC, SiO_2 = 57.96%) and Los Gordos (SiO_2 = 63.2%), which present the lowest values of $\delta^{11}B$ (most depleted) of all the units at Paniri. Malku has a value of $\delta^{11}B$ = -6.11‰, very close to that of depleted mantle and is the only value at Paniri that overlaps with the $\delta^{11}B$ range of the basement granitoids ($\delta^{11}B$ -11 ‰ to -5 ‰, e.g., Kasemann et al., 2000). Malku and Los

Gordos are thought to have been episodes of singular mantle sourced mafic magma escapes which are diverted from the APMB and emplaced in the shallow magma-plumbing systems; these types of occurrences are not rare in the area (Godoy et al., 2018; González-Maurel et al., 2019a).

All the other lava units Laguna, Las Lenguas, Las Negras, Viscscha, and Llareta have $\delta^{11}B$ values of -0.78, -1.29, 0.23, -1.78 and -0.76 ‰ respectively and all have SiO_2 content > 63 wt%, making them intermediate in composition. Such relatively high $\delta^{11}B$ values in arc magma settings are generally thought to require the influence of sources with high $\delta^{11}B$ values as mentioned above.

There is also no strong evidence for a crustal control on boron contents at Paniri, as there is no strong correlation between the boron concentrations with either SiO_2 or measured $^{87}Sr/^{86}Sr$ values (not plotted). There is a weak/almost linear correlation between $\delta^{11}B$ and $^{87}Sr/^{86}Sr$ which suggests a degree of crustal influence on the $\delta^{11}B$ values at Paniri (Figure 17). According to Godoy et al. (2018) AFC is observed in the early-stage processes at Paniri, and this process has the potential to result in different $\delta^{11}B$ values at Paniri, as suggested by Schmitt et al. (2002) for ignimbrite units in the Central Andes. There is a strong correlation however between B vs Nb/B (R^2 = 0.642, Figure 16B) for samples from Paniri suggesting a boron enrichment by slab derived fluids, similar to other arc lava suits (e.g., de Hoog and Savov, 2018, Ishikawa and Tera, 1997, Tonarini et al., 2001a, Zhang et al., 2018, Godoy et al., 2023). The B-Nb/B correlation and the different boron content with differentiation leads to the suggestion that there is variation or heterogeneity in the mantle metasomatism controlling the boron composition at Paniri.

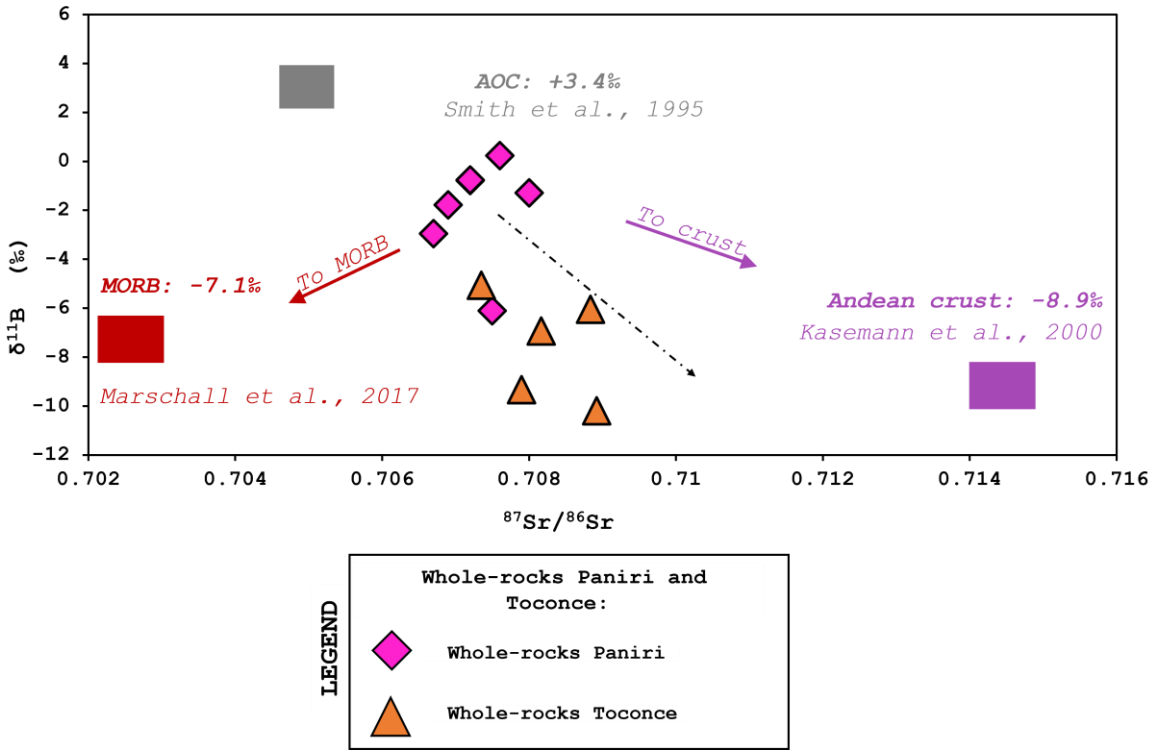

Figure 17. $\delta^{11}B$ vs $^{87}Sr/^{86}Sr$ plot showing crustal influence on δ11B values at Paniri and Toconce.

5.3.2. Toconce B contents and $\delta^{11}B$ values

B concentrations at Toconce vary between 19 and 84 ppm with temporal variation in $\delta^{11}B$ values of erupted magma for each mapped unit and variations between the units varying between -11.16 and -5.06 ‰. Unlike at Paniri where it was difficult to sample for two samples per eruptive unit/lava flow, one sample proximal and another distal from eruption vent, at Toconce it was possible to get two samples per eruptive unit for Lava Turi, Lava Pieneta, and Lava Toconce (Figure 18)).

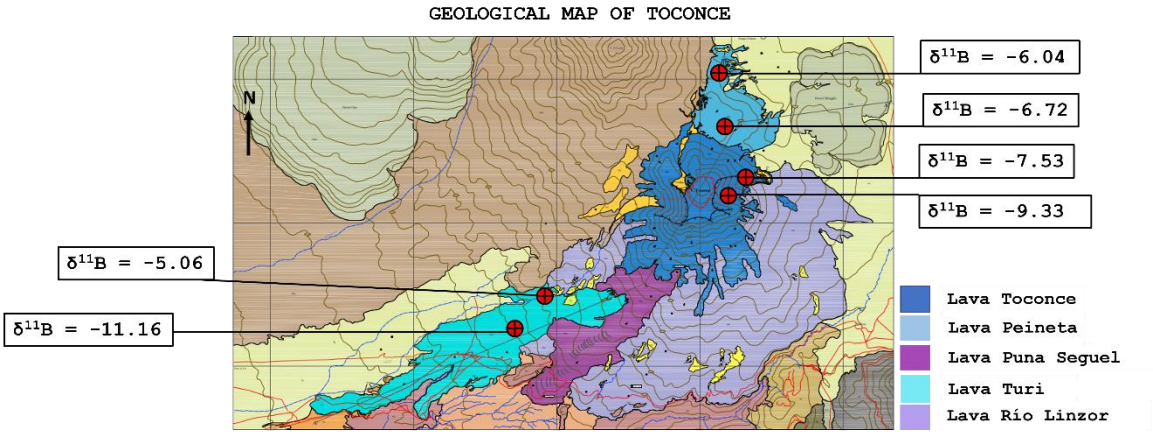

Figure 18. Distribution of samples from the same eruptive unit taken at Toconce.

Within (Intra-unit) each of the three units namely Turi (Figure 18), Pieneta and Toconce (n = 2 samples for each unit) there is an observed consistent variation in the $\delta^{11}B$ and $^{87}Sr/^{86}Sr$ values (Figure 17). The distal samples from these units show values with the lower $\delta^{11}B$ and higher $^{87}Sr/^{86}Sr$ values and the more proximal samples have the higher $\delta^{11}B$ and lower $^{87}Sr/^{86}Sr$ values within each unit, as seen in Figure 19. For $\delta^{11}B$ this could suggest that as magma ascends through the thick crust (and APMB) the easily or first-melted crustal material with most of the B in the crust (basement granitoids and metasediments with $\delta^{11}B$ = -11 to -5 ‰; Kasemann, 2000) are assimilated and progressively depleted, leading to progressively less assimilated B in magmas as the eruption continues. This could explain the $\delta^{11}B$ variation within each unit at Toconce and the influence of erupting magmas in progressively depleting boron components in the crust.

Between units (Inter-unit) at Toconce, the older units, e.g., Lava Rio Linzor, Lava Turi, Lava Puna Seguel and Lava Pieneta show the most contamination with $^{87}Sr/^{86}Sr$ values > 0.7080, and lowest $\delta^{11}B$ values from the oldest units to the youngest indicating a strong influence of time in the evolution of magmas at Toconce. Similar to Paniri, there is a strong B-Nb/B correlation at Toconce (R^2 = 0.654, Figure 16B), suggesting a slab derived boron enrichment, similar to other arc lava suits (e.g., de Hoog and Savov, 2018; Ishikawa and Tera, 1997; Tonarini et al., 2001a, Zhang et al., 2018, Godoy et al., 2023).

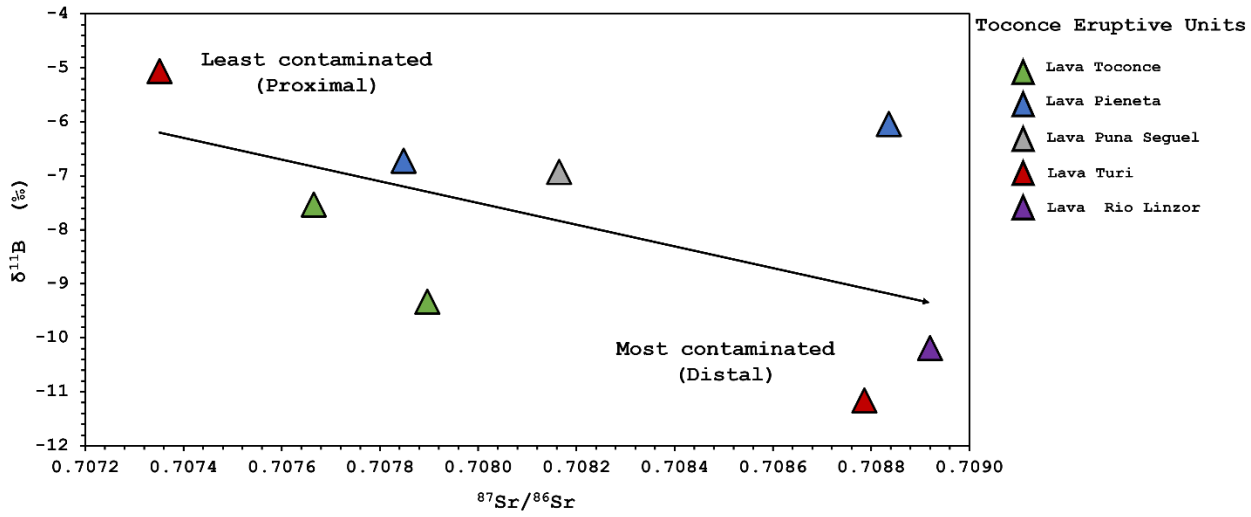

Figure 19. $\delta^{11}B$ vs $^{87}Sr/^{86}Sr$ at Toconce showing Intra- and Inter-unit variations.

5.3.3. Potential influence of crustal assimilation on $\delta^{11}B$ composition of Paniri and Toconce

The San Pedro – Linzor volcanic chain, of which Paniri Toconce are members, has not moved relative to the arc and has remained fixed during its evolution (Polanco et al., 2012), and the boron compositions of Paniri and Toconce cannot be explained by movement of this chain along the arc as proposed by previous $\delta^{11}B$ studies (e.g., Rosner et al. (2003), and Jones et al. (2014)). Other volcanoes along the SPLVC have also remained fixed during the time of their evolution (e.g., González-Maurel et al., 2019b). The location of Toconce relative to Paniri is closer to the centre of the APMB and this is reflected on the heavy $^{87}Sr/^{86}Sr$ values relative to Paniri which is closer to the edges of the APMB, and thus crustal contamination increases towards the centre of the APMB (Godoy et al., 2017; González-Maurel et al., 2019a). An observable trend in Figure 17 is the high $^{87}Sr/^{86}Sr$ values at Toconce associated with low $\delta^{11}B$ values. This is also evidenced in the behavior of the B isotope. There is a progressive depletion from Paniri to Toconce that can be explained by an increased in the degree of interaction between parental magmas and the crust.

An almost positive covariation is observed between $\delta^{11}B$ and $^{87}Sr/^{86}Sr$ for Paniri and a negative correlation for Toconce

(Figure 19Paniri and Toconce experience different assimilation processes as each magma system is fed by a unique magma chamber and at different positions relative to the centre of the APMB. According to Rosner et al., (2003) $\delta^{11}B$ variations in the Central Andean arc are associated with varying degrees of slab derived fluids into the mantle wedge and the distance of the volcanic structures from the arc. We cannot conclude this for Paniri and Toconce volcanoes as the volcanic chain has not moved during the time of their evolution, thus ruling out any volcano-arc geometrical controls.

The effects of crustal contribution in the varying $\delta^{11}B$ values are more pronounced at Toconce than at Paniri. This could be because of the fractional crystallisation of primary magmas during the second stage of evolution (Godoy et al., 2017; González-Maurel et al., 2019a) at Paniri, however this is not well-constrained presently. The $\delta^{11}B$ isotope values at Toconce indicate that as the magma ascends through the thick continental crust, it assimilates first the ^{11}B-depleted crustal component. These values are reflected in the distal (from the volcanic vent) lavas which reflect magmas that first traversed the crust. After this, the more proximal samples (to the vent) reflect magmas from a more slab derived $\delta^{11}B$ source with higher $\delta^{11}B$ values, which traversed the crust later when less of the easily assimilated, ^{11}B-depleted crustal component remained. At Paniri, 5/7 layers with more enriched $\delta^{11}B$ values resemble that of altered oceanic lithosphere, while Malku and Los Gordos, reflect a more depleted mantle value and could result from single magma escapes, a process not rare in the area (Kasemann et al., 2000; Marschall et al., 2017; Godoy et al., 2018).

5.3.4. Modelling $\delta^{11}B$ variations at Paniri and Toconce

In the above section, the effects of crustal assimilation on $\delta^{11}B$ values were explored, ruling out any effect of volcano-arc geometry on these values at Paniri and Toconce. It is also established that $^{87}Sr/^{86}Sr$ values are a good proxy for crustal assimilation (Godoy et al., 2017) and co-vary significantly with $\delta^{11}B$ values, agreeing with Godoy et al. (2023) on this phenomenon observed along the SPLVC. This provides a very constrained petrogenetic framework within which to assess the new B isotope data for Paniri and Toconce.

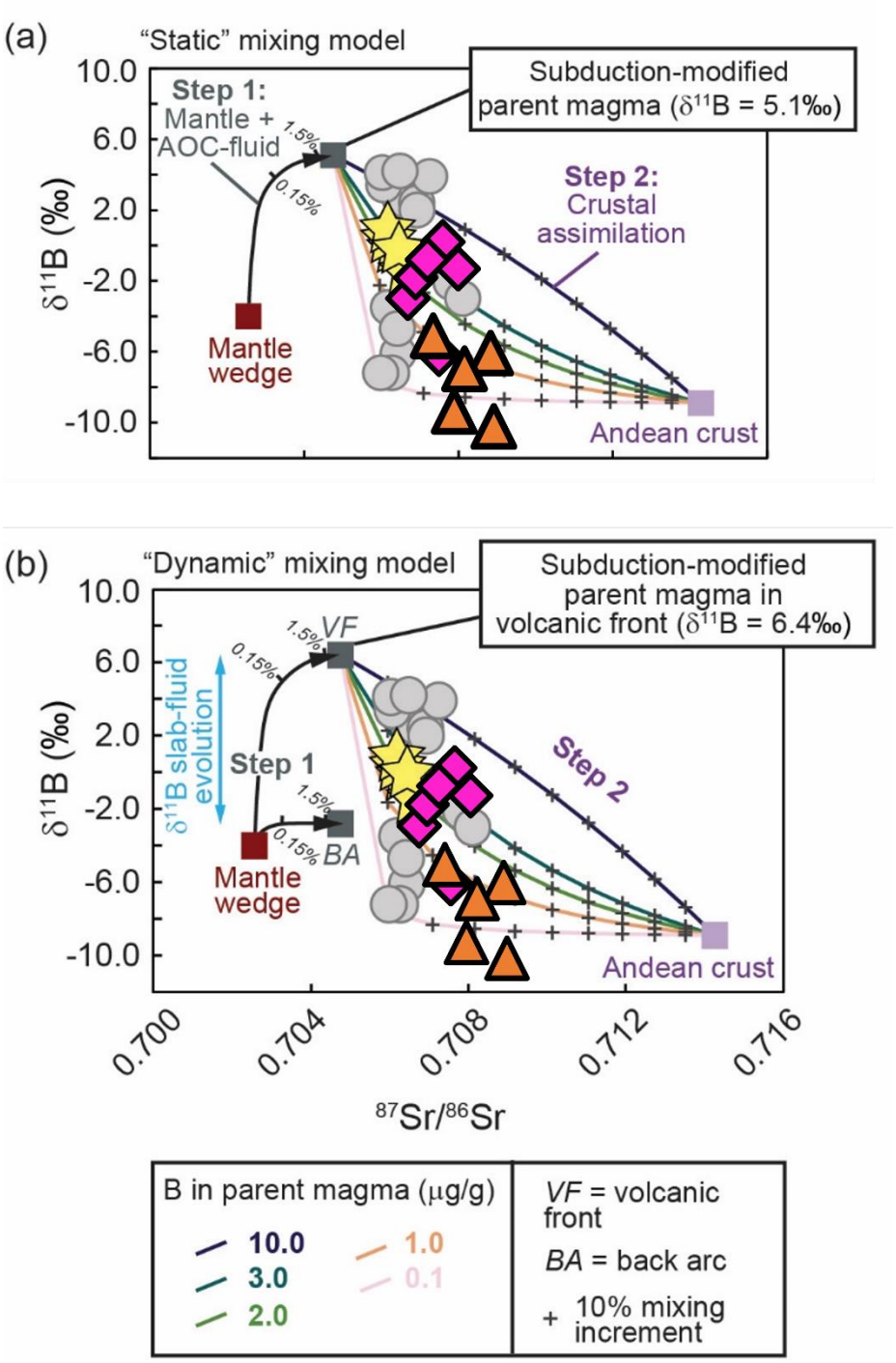

Figure 20. After Godoy et al. (2023) modified modelling from Rosner et al., 2003. (a) B-Sr static and (b) B-Sr dynamic mixing model. Rosner et al. (2003) data plotted as gray circles, and Godoy et al. (2023) La Poruña data plotted as yellow stars, Paniri plotted as pink diamonds and Toconce plotted as orange triangles). In the static mixing model, there is no slab-fluid isotopic fractionation occurring, yielding a subduction-modified parental arc melt with a $\delta^{11}B$ value of +5.1 ‰. In the dynamic mixing model, the $\delta^{11}B$ value of the slab-derived fluid changes as a function of distance from trench, yielding a subduction-modified parental arc melt with $\delta^{11}B$ values between -2.8 ‰ (for addition of back arc fluids; BA) and +6.4 ‰ (for addition of volcanic front fluids; VF). The solid black arrow-lines represent an isotopic

composition of primary arc magmas produced by mixing between the mantle wedge and end-member fluids derived from the subducting slab. The model involves two steps, (1) a primary mantle-like derived melt is mixed with no more than 2% of an AOC-derived slab fluid (mixing curves shown after Rosner et al., 2003). This yields a subduction-modified parental arc melt with $\delta^{11}B$ value between -2.8 ‰ (for addition of back arc fluids; BA) and +6.4 ‰ (for addition of volcanic front fluids; VF). (2) Mixing of the modified parental melt with Andean crust (Godoy et al., 2023).

It is now possible using results from this study to evaluate proposed models of regional B isotope systematics in Andean volcanics using multiple volcanic centres in a single volcanic chain, sampled at the individual unit-level. Rosner et al. (2003) proposed a two-step petrogenetic model to explain the regional B and $\delta^{11}B$ variations in the Central Andes. This model involves three end-members, namely, (1) a slab derived fluid that mainly comes from the AOC component of the Nazca plate, (2) MORB-like asthenospheric mantle wedge, and (3) the continental crust (Rosner et al., 2003). The first step of these mixing models involves an addition of 1.5 wt.‰ of AOC-derived slab fluids to a MORB-like mantle wedge (Tatsumi, 2000), yielding parental melts of arc magmas with $\delta^{11}B$ = -2.8 to +6.4‰. These $\delta^{11}B$ values depend on the consideration of isotopic fractionation across the arc. Following this first step, the second step considered the mixing of the subduction-modified parental arc melts and partial melts of the continental crust, with $\delta^{11}B$ values of about -8.9‰ (Kasemann et al., 2000).

Godoy et al. (2023) (see Figure 5) presented similar B-Sr isotope mixing models for the monogenetic cone La Poruña, which falls just outside of the APMB. The B-Sr isotope data for La Poruña required additional mixing curves to those originally presented by Rosner et al. (2003), indicating that the regional model might not be sufficient for Andean volcanism at the individual volcano level. This was also the case for Paniri and Toconce (Figure 20), to explain the data from these two volcanoes a subduction modified parental arc magma with a relatively high $\delta^{11}B$ value is required. According to the mixing models (Figure 20), Paniri magmas record about 20-30% addition of the Andean continental crust and Toconce magmas record about 25-45% addition of the continental crust, to a subduction modified parental melt with high $\delta^{11}B$ ($\delta^{11}B$ = +5.1 to +6.4‰). Magmas with a high percentage of Andean crust addition (e.g., Paniri and

Toconce) record a relatively low $\delta^{11}B$ value when compared to those with a lower percentage of Andean crust (e.g., La Poruña).

5.4. Regional context for B isotope systematics in Paniri and Toconce

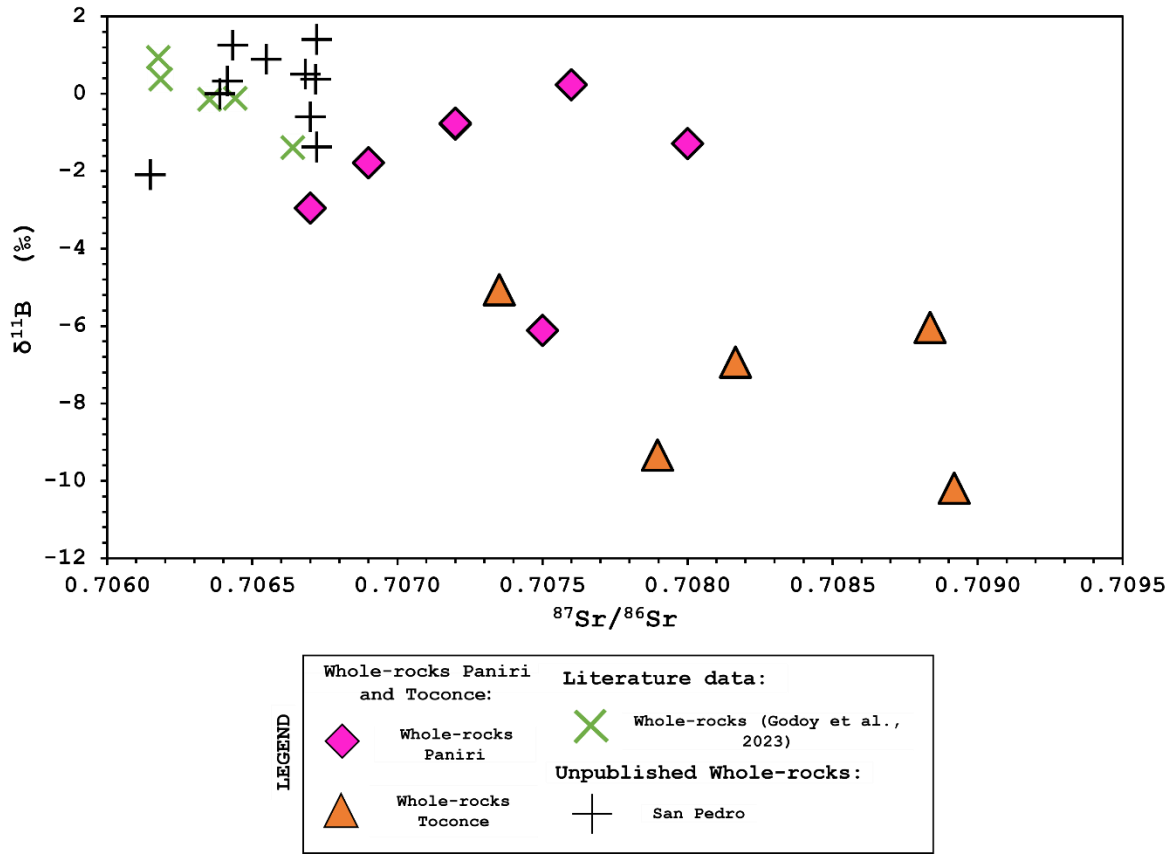

Figure 21. $\delta^{11}B$ vs $^{87}Sr/^{86}Sr$ plot showing crustal influence on δ11B values between two relatively older (i.e., Paniri and Toconce) and two relatively younger (i.e., La Poruña (Godoy et al., 2023), and San Pedro (unpublished)) volcanic centres along the SPLVC.

When comparing the $\delta^{11}B$ data from Paniri and Toconce to those of two relatively younger and less differentiated volcanic centres (González-Maurel et al., 2019a and 2019b, Godoy et al., 2023) in the SPLVC, Paniri and Toconce have more negative $\delta^{11}B$ sources with heavier $^{87}Sr/^{86}Sr$ values. The position of the volcanic centres relative to the AMPB has an influence on the degree of interaction between parental magmas and the old depleted continental crust, and this is highlighted in the Figure 6(Godoy et al., 2014). The younger volcanoes at the edge of the AMPB (i.e., La Poruña and San Pedro) show higher $\delta^{11}B$ values and less

extents of crustal contamination (reflected in Sr-ratios) compared to Paniri and Toconce. This suggests that the source or parental magma for these young volcanoes did not interact with the depleted continental crust as much as Paniri and Toconce source magmas which is reflected in their high $\delta^{11}B$ values and lower $^{87}Sr/^{86}Sr$ values.

Therefore, there is a progressive decrease in crustal assimilation and addition of a ^{11}B-enriched component to magmas in volcanoes from the centre of the APMB towards its edge. This results from modelling the B-Sr (Figure 21) compositional data for Paniri and Toconce agrees with models based on O-Sr data (Figure 14b). The difference is that the ^{11}B-enriched component in the assimilated crust is not constantly available to all magmas during the evolution of these stratovolcanic centres. Unlike the case for oxygen isotopes, this ^{11}B-enriched component is predominantly consumed by magmas transiting the local crust first and progressively less ^{11}B-enriched component is available for later transiting magmas in the same geographical location.

6. Conclusions

Paniri and Toconce basic geochemistry agrees with the SPLVC, a consistent framework

At Paniri SiO_2 values range between 56.04-66.08 wt.% and Na_2O + K_2O from 5.93-7.29 wt.% (andesitic-to-dacitic compositions); while at Toconce SiO_2 range from 56.53-66.08 wt.% and Na_2O + K_2O from 5.25-7.44 wt.% (basaltic-andesite). All comparable to compositions of volcanic centres within the SPLVC. Published and new $^{87}Sr/^{86}Sr$ data at Paniri and Toconce range between 0.7067-0.7079 and 0.7073-0.7089 respectively, showing increased crustal contamination along the SPLVC towards the centre of the APMB. Toconce is geographically located closer to the APMB centre, with higher $^{87}Sr/^{86}Sr$ values compared to Paniri which is closer to the boundary of the APMB. The $\delta^{18}O$ values at Paniri (6.3-8.82 ‰) and Toconce (9.12-10.91 ‰) are higher than the average mantle values (5.5-5.9 ‰), indicating the assimilation of an external source with significantly higher $\delta^{18}O$ values. The increasing $\delta^{18}O$ values, with an increase in SiO_2 and $^{87}Sr/^{86}Sr$ from Paniri to Toconce volcanic centre, confirms the increase in crustal assimilation of the parent magma progressively towards the centre of the APMB.

B-intra (in one flow unit) and inter (between flow units) flow dynamics and the progressive depletion of high-^{11}B component in the crust

The new $\delta^{11}B$ values per eruptive unit at both Paniri and Toconce are higher than the -7.1‰ expected for magmas from the depleted mantle and overlap with Andean basement granitoids and metasediments, which have $\delta^{11}B$ values of -11‰ to -5‰. $\delta^{11}B$ results from two samples per eruptive unit at Toconce show strong evidence of progressive intra-flow enrichment of $\delta^{11}B$ with distal samples reflecting a ^{11}B-depleted compositions compared to samples collected more proximal to the vent.

This trend is also observed between units at both Paniri and Toconce, where the older units have lower δ11B values and the younger units have slightly higher $\delta^{11}B$ values.
At Paniri, part from Las Negras, there is an observed trend from ^{11}B-depleted older eruptive units (Malku $\delta^{11}B$ = -6.11‰) to progressively ^{11}B-enriched younger eruptive units (Llareta $\delta^{11}B$ = -0.76‰). A similar trend is also observed at Toconce, where

older eruptive units are more depleted when compared to the younger eruptive units. The overall observation in the two volcanic centres was that the local ^{11}B-depleted crustal signature gradually decreases with progressive magma eruptions, and the younger eruptive units with more ^{11}B-enriched signatures progressively reflect the higher B composition of the AOC (+3.4 ‰).

This is evidence of a progressive depletion/lowering of magma δ^{11}B values within the crust as magma ascends through the thick crust at Paniri and Toconce. The easily/first melted 11B-depleted crustal material erupt with most of the B contents in the crust as the δ11B reflects basement granitoids and metasediments δ^{11}B values. Gradually, as the eruption events proceed, the δ^{11}B signature approaches the isotopic composition of parental mantle magmas modified by subduction components.

Geographic location of volcanic centres

^{87}Sr/^{86}Sr ratios of volcanic centres along the SPLVC show a notable correlation with the δ^{11}B values in this study and Godoy et al. (2023). The location of the volcanic centres relative to the centre of APMB influences the degree of crustal assimilation of the subduction-modified parental magmas. The enriched δ11B values with relatively lower ^{87}Sr/^{86}Sr values at La Poruña and San Pedro suggest that these magmas had low levels of interaction with the continental crust compared to Paniri and Toconce whose subduction derives parental magma had to ascend through the Andean continental crust and interact with the thick APMB prior to eruption. This observation supports a progressive decrease in crustal assimilation and addition of a ^{11}B-enriched component to magmas in volcanoes as one moves from the centre towards the edges.

Modelled degrees of crustal assimilation based on δ^{11}B

Mixing models based on B and ^{87}Sr/^{86}Sr support a two-step petrogenetic model for B variations at Paniri and Toconce. Step 1, δ^{11}B rich AOC-derived fluids are mixed with a MORB-like mantle wedge resulting in parental melts of arc magmas with 2-3 µg/g at Paniri and 2 µg/g at Toconce, with elevated δ^{11}B values. Step 2, the parental magmas now enriched in δ^{11}B continued to ascend through the thick continental and APMB, assimilating ~20-30 % at Paniri and 25-45 % of the Andean continental crust at Toconce,

and this modifier the $\delta^{11}B$ and $^{87}Sr/^{86}Sr$ ratios. The model aligns with the independently determined degrees of assimilation from O-Sr isotope systematics.

7. References

Acocella, V., Gioncada, A., Omarini, R., Riller, U., Mazzuoli, R. and Vezzoli, L. (2011). Tectonomagmatic characteristics of the back-arc portion of the Calama–Olacapato–El Toro fault zone, Central Andes. *Tectonics*. 30(3).

Aitcheson, S.J., Harmon, R.S., Moorbath, S., Schneider, A., Soler, P., Soria-Escalante, E., Steele, G., Swainbank, I. and Worner, G. (1995). Pb isotopes define basement domains of the Altiplano, central Andes. *Geology*. 23(6):555-558.

Barth, S. (1998). 11B/10B variations of dissolved boron in a freshwater–seawater mixing plume (Elbe Estuary, North Sea). *Marine Chemistry*. 62(1-2):1-14.

Bebout, G.E., Ryan, J.G., Leeman, W.P. and Bebout, A.E. (1999). Fractionation of trace elements by subduction-zone metamorphism—effect of convergent-margin thermal evolution. *Earth and Planetary Science Letters*. 171(1:63-81.

Beck, S.L., Zandt, G., Myers, S.C., Wallace, T.C., Silver, P.G. and Drake, L. (1996). Crustal-thickness variations in the central Andes. *Geology*. 24(5):407-410.

Bindeman, I.N., Ponomareva, V.V., Bailey, J.C. and Valley, J.W. (2004). Volcanic arc of Kamchatka: a province with high-δ18O magma sources and large-scale 18O/16O depletion of the upper crust. *Geochimica et Cosmochimica Acta*. 68(4):841-865.

Burns, D.H., de Silva, S.L., Tepley, F.J. and Schmitt, A.K. (2020). Chasing the mantle: Deciphering cryptic mantle signals through Earth's thickest continental magmatic arc. *Earth and Planetary Science Letters*. 531:115985.

Chaussidon, M. and Marty, B. (1995). Primitive boron isotope composition of the mantle. *Science*. 269(5222):383-386.

Chmielowski, J., Zandt, G. and Haberland, C. (1999). The central Andean Altiplano-Puna magma body. *Geophysical Research Letters*. 26(6):783-786.

Comeau, M.J., Unsworth, M.J. and Ticona, F. (2013). Magnetotelluric images of magma distribution beneath Volcan Uturuncu, Bolivia. *IAVCEI Scientific Assembly. Japan: Kagoshima*.

Damm K.-W., Pichowiak S., Harmon R. S., Todt W., Omarini R., and Niemeyer H. (1990). Pre-Mesozoic Evolution of the Central Andes; The basement revisited. Plutonism from Antarctica to Alaska. *Geological Society of America*. 241:101-126.

Davidson, J. P., McMillan, N. J., Moorbath, S., Wörner, G., Harmon, R. S., and Lopez-Escobar, L. (1990). The Nevados de Payachata volcanic region (18S/69W, N. Chile) II. Evidence for widespread crustal involvement in Andean magmatism. *Contributions to Mineralogy and Petrology*. 105(4):412–432.

Davidson, J.P. and de Silva, S.L. (1992). Volcanic rocks from the Bolivian Altiplano: Insights into crustal structure, contamination, and magma genesis in the central Andes. *Geology*. 20(12):1127-1130.

Davidson, J.P. and de Silva, S.L. (1995). Late cenozoic magmatism of the Bolivian Altiplano. *Contributions to Mineralogy and Petrology*. 119(4):387-408.

De Hoog, J.C. and Savov, I.P. (2018). Boron isotopes as a tracer of subduction zone processes. Boron isotopes: The fifth element. 217-247.

de Silva, S.L. (1989). Altiplano-Puna volcanic complex of the central Andes. *Geology*. *17*(12):1102-1106.

de Silva, S.L., and Francis, P.W. (1991). Volcanoes of the Central Andes. *Springer-Verlag, Heidelberg*. 216.

de Silva, S. L., Self, S., Francis, P., Drake, R., and Carlos, R. (1994). Effusive silicic volcanism in the central Andes: The Chao dacite and other young lavas of the Altiplano-Puna Volcanic Complex. *Journal of Geophysical Research*. 99(B9):17805-17825.

de Silva, S., Zandt, G., Trumbull, R., Viramonte, J.G., Salas, G. and Jiménez, N. (2006). Large ignimbrite eruptions and volcano-tectonic depressions in the Central Andes: a thermomechanical perspective. *Geological Society, London, Special Publications*. 269(1):47-63.

Deegan, F.M., Whitehouse, M.J., Troll, V.R., Geiger, H., Jeon, H., le Roux, P., Harris, C., van Helden, M. and González-Maurel, O. (2021). Sunda arc mantle source δ18O value revealed by intracrystal isotope analysis. Nature Communications, 12(1), p.3930.

Elburg, M.A. (2010). Sources and processes in arc magmatism: The crucial role of water. *Geologica Belgica*. 13:121-136.

Francis, P.W. and Baker, M.C.W. (1977). Mobility of pyroclastic flows. *Nature*. 270(5633):164-165.

Francis, P.W. and De Silva, S.L. (1989). Application of the Landsat Thematic Mapper to the identification of potentially active volcanoes in the Central Andes. *Remote Sensing of Environment*. 28:245-255.

Feeley, T.C. and Sharp, Z.D. (1995). 18O16O isotope geochemistry of silicic lava flows erupted from Volcán Ollagüe, Andean Central Volcanic Zone. *Earth and Planetary Science Letters*. 133(3-4):239-254.

Gill, J. B. (1981). Orogenic Andesites and Plate Tectonics. *Springer-Verlag, New York*. 390.

Godoy, B., Wörner, G., Kojima, S., Aguilera, F., Simon, K., and Hartmann, G. (2014). Lowpressure evolution of arc magmas in thickened crust: The San Pedro-Linzor volcanic chain, Central Andes, Northern Chile. *Journal of South American Earth Sciences*. 52:24-42.

Godoy, B., Wörner, G., Le Roux, P., de Silva, S., Parada, M.Á., Kojima, S., González-Maurel, O., Morata, D., Polanco, E. and Martínez, P. (2017). Sr-and Nd-isotope variations along the Pleistocene San Pedro–Linzor volcanic chain, N. Chile: Tracking the influence of the upper crustal Altiplano-Puna Magma Body. *Journal of Volcanology and Geothermal Research*. 341:172-186.

Godoy, B., Lazcano, J., Rodríguez, I., Martínez, P., Parada, M.A., Le Roux, P., Wilke, H.G. and Polanco, E. (2018). Geological evolution of Paniri volcano, central Andes, northern Chile. *Journal of South American Earth Sciences*. 84-184-200.

Godoy, B., Taussi, M., González-Maurel, O., Renzulli, A., Hernández-Prat, L., le Roux, P., Morata, D. and Menzies, A. (2019). Linking the mafic volcanism with the magmatic stages during the last 1 Ma in the main volcanic arc of the Altiplano-Puna Volcanic Complex (Central Andes). *Journal of South American Earth Sciences*. 95-102295.

Godoy, B., Deegan, F.M., González-Maurel, O., le Roux, P., Garbe-Schönberg, D., Rodríguez, I., Guzmán-Marusic, G. and Marín, C. (2023). Boron isotope variations in a single monogenetic cone: La Poruña (21° 53′ S, 68° 30′ W), Central Andes, Chile. *Lithos*. 440:107030.

González-Maurel, O., le Roux, P., Godoy, B., Troll, V.R., Deegan, F.M. and Menzies, A. (2019a). The great escape: Petrogenesis of low-silica volcanism of Pliocene to Quaternary age associated with the Altiplano-Puna Volcanic Complex of northern Chile (21 10′-22 50′ S). *Lithos*. 346-347:105162.

González-Maurel, O., Godoy, B., Le Roux, P., Rodríguez, I., Marín, C., Menzies, A., Bertin, D., Morata, D. and Vargas, M. (2019b). Magmatic differentiation at La Poruña scoria cone, Central Andes, northern Chile: Evidence for assimilation during turbulent ascent processes, and genetic links with mafic eruptions at adjacent San Pedro volcano. *Litho.* 338-339:128-140.

González-Maurel, O., Deegan, F.M., le Roux, P., Harris, C., Troll, V.R., and Godoy, B. (2020). Constraining the sub-arc, parental magma composition for the giant Altiplano-Puna Volcanic Complex, northern Chile. *Scientific Reports*. 10(1):6864.

Goss, A.R. and Kay, S.M. (2009). Extreme high field strength element (HFSE) depletion and near-chondritic Nb/Ta ratios in Central Andean adakite-like lavas (~28 S, ~68 W). *Earth and Planetary Science Letters*, 279(1-2):97-109.

Gottsmann, J., Blundy, J., Henderson, S., Pritchard, M.E. and Sparks, R.S.J. (2017). Thermomechanical modeling of the Altiplano-Puna deformation anomaly: *Multiparameter insights into magma mush reorganization. Geosphere*. 13(4):1042-1065.

Grove, T.L., Till, C.B. and Krawczynski, M.J. (2012). The role of H2O in subduction zone magmatism. *Annual Review of Earth and Planetary Sciences*. 40:413-439.

Grunder, A.L., Thompson, J.M., and Hildreth, W. (1987). The hydrothermal system of the Calabozos caldera, central Chilean Andes. *Journal of Volcanology and Hydrothermal Research*. 32: 287-298.

Hemming, N.G. and Hanson, G.N. (1992). Boron isotopic composition and concentration in modern marine carbonates. *Geochimica et Cosmochimica Acta*. *56*(1):537-543.

Hoog, J., De, C.M. and Savov, I.P. (2018). Boron isotopes as a tracer of subduction zone processes. *Boron Isotopes*. 217-247.

Isacks, B.L. (1988). Uplift of the central Andean plateau and bending of the Bolivian orocline. *Journal of Geophysical Research: Solid Earth*. *93*(B4):3211-3231.

Ishikawa, T. and Nakamura, E. (1993). Boron isotope systematics of marine sediments. *Earth and Planetary Science Letters*. 117(3-4):567-580.

Ishikawa, T. and Tera, F. (1997). Source, composition and distribution of the fluid in the Kurile mantle wedge: constraints from across-arc variations of B/Nb and B isotopes. *Earth and Planetary Science Letters*. 152(1-4):123-138.

Iovine, R.S., Mazzeo, F.C., Arienzo, I., D'Antonio, M., Wörner, G., Civetta, L., Pastore, Z. and Orsi, G. (2017). Source and magmatic evolution inferred from geochemical and Sr-O-isotope data on hybrid lavas of Arso, the last eruption at Ischia Island (Italy; 1302 AD). *Journal of Volcanology and Geothermal Research*. 331:1-15.

James, D.E. (1971). Andean crustal and upper mantle structure. *Journal of Geophysical Research*. 76(14-3246-3271.

Jones, R.E., De Hoog, J.C., Kirstein, L.A., Kasemann, S.A., Hinton, R., Elliott, T. and Litvak, V.D. (2014). Temporal variations in the influence of the subducting slab on Central Andean arc magmas: Evidence from boron isotope systematics. *Earth and Planetary Science Letters*. 408:390-401.

Kasemann, S., Erzinger, J. and Franz, G. (2000). Boron recycling in the continental crust of the central Andes from the Palaeozoic to Mesozoic, NW Argentina. *Contributions to Mineralogy and Petrology*. 140(3):328-343.

Leeman, W.P. and Sisson, V.B. (1996). Geochemistry of boron and its implications for crustal and mantle processes. *Reviews in Mineralogy and Geochemistry*. 33(1):645-707.

Lindsay, J.M., de Silva, S., Trumbull, R., Emmermann, R. and Wemmer, K. (2001). La Pacana caldera, N. Chile: a re-evaluation of the stratigraphy and volcanology of one of the world's largest resurgent calderas. Journal of Volcanology and Geothermal Research, 106(1-2):145-173.

Lister, J. (2019). Petrogenesis of lavas from Volcano Azufre, Northern Chile: evidence for crustal input. Dissertation, MSc. Thesis, University of Cape Town, South Africa.

López, C., Aguilera, F., Godoy, B., Wörner, G. and Kojima, S. (2012). Evolución del sistema Volcánico Toconce (Región de Antofagasta, Chile) mediante interpretación fotogeológica, petrográfica y geoquímica. In *XII Congreso Geológico Chileno, Antofagasta, Chile.* Vol. 4:594-596.

Mamani, M., Tassara, A. and Wörner, G. (2008). Composition and structural control of crustal domains in the central Andes. *Geochemistry, Geophysics, Geosystems*. *9*(3).

Mamani, M., W□orner, G., and Sempere, T. (2010). Geochemical variations in igneous rocks of the Central Andean orocline (13S to 18S): Tracing

crustal thickening and magma generation through time and space. *Bulletin of the Geological Society of America*. 122(1-2):162-182.

Marinovic, N. and Lahsen, A. (1984). Hoja Calama, Región de Antofagasta: escala 1: 250.000.

Marrett, R. and Strecker, M.R. (2000). Response of intracontinental deformation in the central Andes to late Cenozoic reorganization of South American Plate motions. *Tectonics*. 19(3):452-467.

Marschall, H.R. and Schumacher, J.C. (2012). Arc magmas sourced from mélange diapirs in subduction zones. *Nature Geoscience*. *5*(12):862-867.

Marschall, H.R. (2018). Boron isotopes in the ocean floor realm and the mantle. *Boron isotopes*. 189-215.

Marschall, H.R. and Foster, G.L. (2018). Boron isotopes in the earth and planetary sciences — a short history and introduction. *Boron Isotopes: The Fifth Element.* 1-11.

Mattey, D., Lowry, D. and Macpherson, C. (1994). Oxygen isotope composition of mantle peridotite. *Earth and Planetary Science Letters*. 128(3-4):231-241.

Michelfelder, G.S., Feeley, T.C., Wilder, A.D. and Klemetti, E.W. (2013). Modification of the continental crust by subduction zone magmatism and vice-versa: Across-strike geochemical variations of silicic lavas from individual eruptive centers in the Andean Central volcanic zone. *Geosciences*. 3(4):633-667.

Morris, J.D., Leeman, W.P. and Tera, F. (1990). The subducted component in island arc lavas: constraints from Be isotopes and B–Be systematics. *Nature*. *344*(6261):31-36.

Murphy, J.B. (2006). Igneous rock associations 7. Arc magmatism I: relationship between subduction and magma genesis. *Geoscience Canada*. 33(4):145-168.

Palmer, M.R. (1991). Boron-isotope systematics of Halmahera arc (Indonesia) lavas: evidence for involvement of the subducted slab. *Geology*. *19*(3):215-217.

Peacock, S.M. and Hervig, R.L. (1999). Boron isotopic composition of subduction-zone metamorphic rocks. *Chemical Geology*. 160(4):281-290.

Plank, T. (2014). The chemical composition of subducting sediments. *Elsevier*.

Polanco, E., Clavero, J. and Giavelli, A. (2012). Geología de la cadena volcánica Paniri-Toconce, Zona Volcánica Central, Altiplano de la Región de Antofagasta, Chile. In *XII Congreso Geológico Chileno, Antofagasta, Chile*. Vol. 4:462-464.

Pritchard, M.E., De Silva, S.L., Michelfelder, G., Zandt, G., McNutt, S.R., Gottsmann, J., West, M.E., Blundy, J., Christensen, D.H., Finnegan, N.J. and Minaya, E. (2018). Synthesis: PLUTONS: Investigating the relationship between pluton growth and volcanism in the Central Andes. *Geosphere*. 14(3):954-982.

Prezzi, C.B., Götze, H.J. and Schmidt, S. (2009). 3D density model of the Central Andes. *Physics of the Earth and Planetary Interiors*. *177*(3-4):217-234.

Ramos, V.A. (2008). The basement of the Central Andes: the Arequipa and related terranes. *Annu. Rev. Earth Planet. Sci.* 36:289-324.

Riller, U., Petrinovic, I., Ramelow, J., Strecker, M. and Oncken, O. (2001). Late Cenozoic tectonism, collapse caldera and plateau formation in the central Andes. *Earth and Planetary Science Letters*. 188(3-4):299-311.

Rosner, M., Erzinger, J., Franz, G. and Trumbull, R.B. (2003). Slab-derived boron isotope signatures in arc volcanic rocks from the Central Andes and evidence for boron isotope fractionation during progressive slab dehydration. *Geochemistry, Geophysics, Geosystems*. *4*(8).

Schmitt, A., De Silva, S., Trumbull, R. and Emmermann, R. (2001). Magma evolution in the Purico ignimbrite complex, northern Chile: evidence for zoning of a dacitic magma by injection of rhyolitic melts following mafic recharge. *Contributions to Mineralogy and Petrology*. 140:680-700.

Seelenfreund, A., Fonseca, E., Llona, F., Lera, L., Sinclaire, C. and Rees, C. (2009). Geochemical analysis of vitreous rocks exploited during the Formative Period in the Atacama Region, Northern Chile. *Archaeometry*. *51*(1):1-25.

Sigauke, C. (2022). Why are there no low-δ18O magmas in convergent margins? A case of the Central Andes, Northern Chile. Dissertation, MSc. Thesis, University of Cape Town, South Africa.

Smith, H.J., Spivack, A.J., Staudigel, H. and Hart, S.R. (1995). The boron isotopic composition of altered oceanic crust. *Chemical Geology*. 126(2):119-135.

Spivack, A.J. and Edmond, J.M. (1987). Boron isotope exchange between seawater and the oceanic crust. *Geochimica et Cosmochimica Acta*. *51*(5):1033-1043.

Stern, C.R. (1991). Role of subduction erosion in the generation of Andean magmas. *Geology* 19:78-81.

Stern, R.J., 2002. Subduction zones. Reviews of geophysics, 40(4), pp.3-1.

Stern, C.R. (2004). Active Andean volcanism: its geologic and tectonic setting. *Revista geológica de Chile*. 31(2):161-206.

Stern, C.R., Moreno, H., López-Escobar, L., Clavero, J.E., Lara, L.E., Naranjo, J.A., Parada, M.A. and Skewes, M.A. (2007). *Chilean volcanoes*.

Tatsumi, Y., Hamilton, D.L. and Nesbitt, R.W. (1986). Chemical characteristics of fluid phase released from a subducted lithosphere and origin of arc magmas: evidence from high-pressure experiments and natural rocks. *Journal of Volcanology and Geothermal Research*. 29(1-4):293-309.

Tatsumi, Y. and Eggins, S. (1995). *Subduction zone magmatism* (Vol. 1). *Wiley*.

Tatsumi, Y. (2000). Continental crust formation by crustal delamination in subduction zones and complementary accumulation of the enriched mantle I component in the mantle. *Geochemistry, Geophysics, Geosystems*. 1(12).

Tonarini, S., Leeman, W.P. and Leat, P.T. (2011). Subduction erosion of forearc mantle wedge implicated in the genesis of the South Sandwich Island (SSI) arc: evidence from boron isotope systematics. *Earth and Planetary Science Letters*. 301(1-2):275-284.

Trumbull, R.B., Wittenbrink, R., Hahne, K., Emmermann, R., Büsch, W., Gerstenberger, H. and Siebel, W. (1999). Evidence for Late Miocene to Recent contamination of arc andesites by crustal melts in the Chilean Andes (25–26 S) and its geodynamic implications. *Journal of South American Earth Sciences*. 12(2):135-155.

Turner, S., Tonarini, S., Bindeman, I., Leeman, W.P. and Schaefer, B.F., 2007. Boron and oxygen isotope evidence for recycling of subducted components over the past 2.5 Gyr. *Nature*. 447(7145):702-705.

Walowski, K.J., Kirstein, L.A., De Hoog, J.C.M., Elliott, T., Savov, I.P. and Jones, R.E. (2021). Boron recycling in the mantle: Evidence from

a global comparison of ocean island basalts. *Geochimica et Cosmochimica Acta*. 302:83-100.

Ward, K.M., Zandt, G., Beck, S.L., Christensen, D.H. and McFarlin, H. (2014). Seismic imaging of the magmatic underpinnings beneath the Altiplano-Puna volcanic complex from the joint inversion of surface wave dispersion and receiver functions. *Earth and Planetary Science Letters*. 404:43-53.

Wittenbrink, J., Lehmann, B., Wiedenbeck, M., Wallianos, A., Dietrich, A. and Palacios, C. (2009). Boron isotope composition of melt inclusions from porphyry systems of the Central Andes: a reconnaissance study. *Terra Nova*. 21(2):111-118.

Wörner, G., Harmon, R.S., Davidson, J., Moorbath, S., Turner, D.L., McMillan, N., Nyes, C., Lopez-Escobar, L. and Moreno, H. (1988). The nevados de payachata volcanic region (18 S/69 W, N. Chile). *Bulletin of Volcanology*. 50(5):287-303.

You, C.F., Spivack, A.J., Gieskes, J.M., Rosenbauer, R. and Bischoff, J.L. (1995). Experimental study of boron geochemistry: implications for fluid processes in subduction zones. *Geochimica et Cosmochimica Acta*. 59(12):2435-2442.

Yuan, X., Sobolev, S.V. and Kind, R. (2002). Moho topography in the central Andes and its geodynamic implications. *Earth and Planetary Science Letters*. *199*(3-4):389-402.

Zandt, G., Leidig, M., Chmielowski, J., Baumont, D. and Yuan, X. (2003). Seismic detection and characterization of the Altiplano-Puna magma body, central Andes. *Pure and Applied Geophysics*. 160(3):789-807.

Zhao, K.D., Jiang, S.Y., Nakamura, E., Moriguti, T., Palmer, M.R., Yang, S.Y., Dai, B.Z. and Jiang, Y.H. (2011). Fluid–rock interaction in the Qitianling granite and associated tin deposits, South China: evidence from boron and oxygen isotopes. *Ore Geology Reviews*. 43(1):243-248.